Force-Guided Assembly Using Tuned Dither and Recursive Parameter Estimation

by

Susan L. Ipri

BSE, Mechanical and Aerospace Engineering (1993)
Princeton University

Submitted to the Department of Mechanical Engineering

in Partial Fulfillment of the Requirements for the degree of

Master of Science in Mechanical Engineering

at the

Massachusetts Institute of Technology

February, 1995

©Massachusetts Institute of Technology 1995
All rights reserved

Signature of Author ______________________________
Department of Mechanical Engineering
February 10, 1995

Certified by ______________________________
Dr. Haruhiko Asada
Professor
Thesis Supervisor

Accepted by ______________________________
Dr. Ain A. Sonin
Chairman, Department Committee on Graduate Students

ARCHIVES
MASSACHUSETTS INSTITUTE
OF TECHNOLOGY

APR 06 1995

Force-Guided Assembly Using Tuned Dither and Recursive Parameter Estimation

by
Susan L. Ipri

Submitted to the Department of Mechanical Engineering
on February 10, 1995 in partial fulfillment of the
requirements for the Degree of Master of Science in
Mechanical Engineering

ABSTRACT

A novel approach to force-guided robotic assembly which combines friction suppression and force feedback parameter estimation is presented. Preliminary development work for this algorithm, called active force sensing, indicates its feasibility and distinct advantages for real-time control. Friction is a major source of error and noise for robotic operation, and due to a strong dependence on environmental and dynamic parameters, it is extremely hard to model and predict. Knowledge of the dynamics of the friction phenomenon help to define a high frequency, low amplitude dither signal. This dither, added to the robot end point motion, maintains the assembly parts in relative motion, whereby reducing the friction forces generated. Also, the parameters of the dither are tuned based on the force output to further minimize the frictional effects.

A force feedback parameter estimation scheme is also outlined for on-line control of robotic assembly tasks in uncertain environments. With minimized friction effects, the feedback force signals are more accurately interpreted, and errors and unknown parameters are more easily detected and compensated for. A lower frequency dither initiated at a point on the surface allows for the determination of the localized tangent based on manipulation of the resulting force measurements. The two operations approach force feedback and friction suppression from a dynamic perspective, allowing for improved flexibility in control and control parameter selection. The result is a promising new control system for robotic assembly in unknown environments.

Thesis Advisor: Dr. Haruhiko Asada

Title: Professor of Mechanical Engineering

ACKNOWLEDGEMENTS

A wise man and good friend once gave me a sheet that read

> *You alone can do it,*
> *but you can't do it alone.*

I can't think of more fitting words with which to begin my acknowledgements.

My friends and family have always been supportive of my work, and their continual interest and humor keeps me going through good and bad days alike. Grandpop especially, you'll always be the first engineer of the family and a shining example I'm proud to follow. I feel extremely lucky to have your support and love.

All the guys in lab were always there to answer questions no matter how small, Sooyong, Xiang-Dong, Kevin, Anton, BooHo, Danny, Mark, Samir, Ming, Ken, Toi, Nori and Nakashima. My advisor, Professor Asada, provided me with excellent guidance, allowing me the space to think for myself and recognize what it takes to do quality research.

And Caryl, all those times you waited to walk me home, all the errands you ran for me, all the jokes you timed just right, and all your love was just what I needed to keep my spirits and determination high.

Thanks.

Support for this project is provided by the National Science Foundation under grant IRI931888 and the Advanced Research Projects Agency.

Contents

1 INTRODUCTION **13**
1.1 Scope of Thesis 13
1.2 Background 14
1.3 The Dither Operation 15
1.4 Task Applicability 16
1.5 Organization of Thesis 16

2 LITERATURE REVIEW **17**
2.1 Dither 17
2.2 Friction 18
2.3 Control Techniques for Robotic Assembly 18
2.4 Task Planning and Surface Tracking 19

3 MODELING **21**
3.1 Physical System 21
3.2 Hybrid Control 22

4 FRICTION SUPPRESSION **25**
4.1 The Basis for Friction Suppression 25
4.2 Friction Model 26
4.3 The Effect of Dither on Friction Forces 28
4.4 Dither Tuning 31
  4.4.1 Existence of An Optimal Parameter Set 31
  4.4.2 Parameter Update Law 32
4.5 Verification and Experimentation 33
  4.5.1 Experimental Set-Up 33
  4.5.2 Experimentation 34

5 SURFACE TRACKING **41**
5.1 Surface Tracking Through Parameter Estimation 41
5.2 Preliminary Studies 42
5.3 Estimation of Surface Tangent Using Dither 44
  5.3.1 Contact Models 45
  5.3.2 Theoretical Model 46
  5.3.3 Simulation 48

5.4 Multiple Point Contact Manipulation 48
    5.4.1 Multiple Point Contact Assembly 49
    5.4.2 Theoretical Framework 51
    5.4.3 Simulation 53

6 ACTIVE FORCE SENSING 55
6.1 Contributions of Tuned Dither for Friction Suppression 55
6.2 Analysis of Force Feedback Algorithm 56
    6.2.1 Assumptions 56
    6.2.2 Validity 58
6.3 A Successful Combination 58

7 CONCLUSIONS AND FUTURE RECOMMENDATIONS 61
7.1 Conclusions 61
7.2 Future Recommendations 61

List of Figures

1.1 Active Force Sensing 14

3.1 Typical Assembly Task 22
3.2 Dynamic System Model 22
3.3 Coordinate Reference Frames 23
3.4 Hybrid Position/Force Control 24

4.1 Individual Friction Components 27
4.2 General Form of the Friction/Velocity Curve 28
4.3 Friction Force for Periodic Dither Signal 29
4.4 Friction Force for a Nominal Velocity and Dither Operation 30
4.5 Friction Forces with and without Dither 35
4.6 Variation of Tangential Force with Normal Force and Determination of μ 36
4.7 Change in Signal Oscillation Magnitude with Dither Amplitude . . . 37
4.8 Tuning of Dither Amplitude 38
4.9 Tuning of Dither Amplitude 38
4.10 Tuning of Dither Amplitude 39

5.1 Use of Dither for One Dimensional Trajectories 42
5.2 Successful Dither Estimation of A Quadratic Function 44
5.3 Poor Dither Correlation from unknown Initial Conditions and Discrete Changes 45
5.4 Single-Point Contact Model 46
5.5 Dither Operation in the Task Space 47
5.6 Simulation of Surface Tracking for Sinusoidal Function 49
5.7 Multiple-Point Contact Model 50
5.8 Construction of Dither Axes 52
5.9 Simulation of Multiple Point Contact Assembly - Rotation of Box into Corner 54
5.10 Actual versus Estimated Point of Instantaneous Rotation 54

List of Symbols

$\dot{x}$: Actual robot velocity
$\dot{x}_o$: Nominal robot velocity
d : Dither signal
$\hat{d}$: Nominal dither value
A : Dither amplitude
ω : Dither frequency
k_e : Interaction stiffness
b_e : Interaction damping
X, Y : Inertial reference frame coordinates
x_e, y_e : End effector reference frame coordinates
x, y : Task reference frame coordinates
R : Hybrid controller selection matrix
F_f : Total friction force
F_{static} : Static friction force
k_{fric} : Static friction characteristic stiffness
F_t : Kinetic friction coefficient
$sgn(y)$: Sign of y, $\frac{y}{abs(y)}$
F_N : Normal contact force
μ : Coefficient of sliding friction
F_s : Stribeck friction coefficient
$\dot{x}_s$: Stribeck friction characteristic velocity
F_v : Velocity dependent friction coefficient
$\bar{F}_f$: Average friction force
λ : Constant friction term
J : Dither tuning cost function
$()_{opt}$: Optimal value
σ_f^2 : Standard deviation of force signal
T : Dither period
t : Tangential direction
n : Normal direction
$\hat{}$: Estimate
α_o : Error in tangent angle
$\delta\alpha$: Dither angle
F_{fs} : Force sensor output
RMS : Root Mean Square
P : Instantaneous center of rotation
k_x : Stiffness in x-direction
F_T : Force in tangential direction, non friction discussions
M_s : Measured torques from force sensor
M_p : Moment about the instantaneous center of rotation

Chapter 1

INTRODUCTION

1.1 Scope of Thesis

This thesis develops the fundamental control subprocesses required for successful robotic assembly control in uncertain environments. These subprocesses consist of the development of a friction suppression algorithm, including an understanding of the friction properties of a dynamic system, and a technique for interpreting force readings in the context of robotic assembly tasks. These subprocesses are intended to support a new technique, active force sensing, which unites a friction suppression algorithm with a force feedback parameter estimation scheme shown in Figure 1.1. The combination produces a control strategy which automatically accounts for error and uncertainties in the task operation while minimizing the detrimental effect of friction on the force feedback. With these two subprocesses completed, the application of active force sensing can succeed. For widest applicability, active force sensing aims to achieve a control structure which inflicts the least interaction on the task parts. The goal is to maintain contact between the robot and its environment with the least contact force and minimal friction force. Minimal contact reduces the possible harmful effects of large forces between sensitive parts, requires less control action, and produces less resistance to motion. Friction suppression is aided by such minimization and in turn the friction suppression allows for a smoother task operation. Active force sensing is based on this synergy.

An effective friction suppression algorithm must incorporate the underlying physical nature of the friction phenomenon, allowing for variation in robot speed and environmental properties. Friction suppression is achieved through the addition of a high frequency dither which maintains the assembly parts in relative motion and eliminates the occurrence of stiction. Likewise, through a characterization of the physical nature of the friction, the dither parameters can be adjusted on-line to further minimize the friction forces.

Force feedback signals, which contain much information about a given dynamic interaction, are only effective if they are properly interpreted in the context of the task. For robotic assembly, a relationship is explored between the force measurements and the relative orientation of a robot end effector to the environment. Estimation of

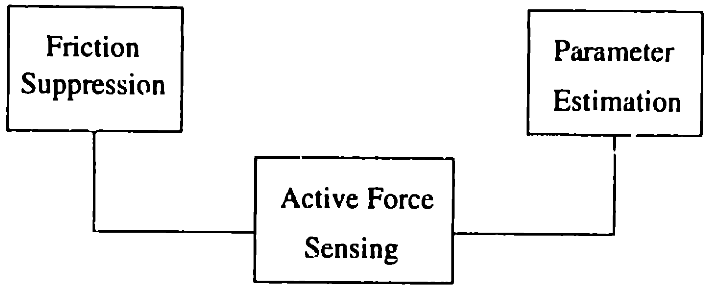

Figure 1.1: Active Force Sensing

this orientation allows the robot assembly task trajectory to be accurately updated.

The work presented in this thesis is discussed in the context of a surface tracking process for which the robot makes contact with its environment at one or more points. Only continuous sections of the surface are considered, assuming no singularities exist within a given work range. The end effector tip and surface vary in roughness, and an initial estimate of the admissible motion space is assumed. The geometry of the parts involved are known, yet the exact nature of the environment is not except to the level of a specific task goal being defined.

1.2 Background

The manufacturing industry continually strives to become more and more automated in an effort to decrease assembly time, increase productivity, and increase repeatability of operations. Currently, many robotic automation systems have been placed in manufacturing plants, to perform a range of tasks. In many cases, however, the robot is preprogrammed to execute a single command structure, relying on other systems along the assembly line to ensure that the parts are correctly aligned and delivered on time, or employ visual sensors for on-line adjustment. Such methods to adjust on-line to uncertainties or errors within the system are limited. They usually consist of passive compliance techniques, effective for only a limited range of kinematic configurations, or rely on measurements which do not directly reflect the dynamic states of the control operation. Therefore the need exists for a robust general robotic assembly control structure which has the ability to actively adjust to uncertain conditions within the work environment in an active and useful manner.

Many control techniques are present in the literature, yet few are utilized on the plant floor. Sophisticated techniques are limited by unsatisfactory reliability, calculational intensity, and limited flexibility of the developed assembly techniques. To improve reliability and accuracy in assembly operations, in-process monitoring and closed-loop control are effective tools. Force feedback from contact between mating parts is the major source of information directly related to the assembly process state.

Therefore, the force information is indispensable for closed-loop assembly process control as well as for in-process monitoring.

One disadvantage to force feedback is that the force information reflects not only the dynamics and states of the system, but also friction and stick/slip effects. Accurate force measurements require a filter or active technique to account for each of these elements. An active friction suppression is only effective if it correctly incorporates the underlying physics of the contact interaction. The algorithm should result in controlled, measureable forces, and does not need to completely compensate for the effects of friction. Much previous study has been conducted to model and/or eliminate adverse friction effects. Therefore, very accurate physical models exist for describing the relationship between friction forces and relative velocity. These models must be reinterpreted in the context of active force sensing.

Performing assembly tasks involves a combination of many simple, clearly defined functions including contact detection, surface following, manipulation, and insertion. Any robotic automation system must have the ability to perform each of these tasks prior to completing more complex operations. Surface tracking is especially useful for manipulation of several parts with respect to one another. Tracking requires the determination of the relative orientation of the parts, and for success in uncertain environments, must be formulated in general terms of the contact states.

1.3 The Dither Operation

The use of controlled perturbations, or dither, forms the central mechanism for achieving both friction suppression and parameter estimation. Sinusoidal dither signals can be added open-loop or closed-loop into the robot motion controller, can vary in amplitude and frequency, and have the advantage of periodicity and continuity of form which can be manipulated to form concise, powerful mathematical formulations.

The dither operation consists of superimposing a periodic signal about a nominal control command value. Usually this periodic signal is sinusoidal with a prescribed amplitude and frequency.

$$d = \bar{d} + A \sin \omega t \tag{1.1}$$

where $\bar{d}$ represents the nominal value about which the dither occurs. Usually the relative phase of the dither is not relevant as long as direct measurement of the robot motion is available. The dither is applied with very small amplitudes relative to the overall motion, and much information can be collected with minimal motion and time. With the ability to choose the orientation of the motion, combining more than one dither operations allows an entire localized region to be explored. The persistent excitation condition, which specifies that in order to estimate all the states of a system each degree of freedom of the state space must be explored, can be easily satisfied.

1.4 Task Applicability

The usefulness of any assembly control system depends on its range of applications. Active force sensing is intended for any process which requires monitoring of the relative orientation of parts, accurate tracking, surface following, and/or assembly in uncertain or error-prone environments. Specific applications include connector mating on printed circuit board test stands, manipulation of a vehicle door panel into its frame, or assembly of pocket pager cases. Often minor errors such as small burrs from rough finishes, or misconnections between electrical parts can cause task failures. Active force sensing can adjust for these unpredicted occurrences, and prevent unnecessary assembly and testing failures. Even for repetitive task applications, adaptive systems such as this will allow for compensation of errors.

Many of the assembly tasks which industry intends to automate are also currently performed by human operators. An understanding of the heuristics used by those operators aids in formulating each step of the process control. For example, a human operator will involuntarily wiggle two parts which he or she is having trouble fitting together. Use of the dither operation for robotic assembly captures the human tendency to 'wiggle' parts to aid in manipulating them. This wiggle actually allows the person to explore the local region about the point of contact of his or her part, and discover the path of least resistance. The dither operation similarly determines an optimal direction of motion from an active search of a localized region. Likewise, the operator will be alerted to potential problems in completing his or her task if he or she feels reaction forces which vary from those expected. Much work is currently underway in the field of tactile sensing. Studies have identified microscopic, very high frequency oscillations within the nervous system of the skin and in some cell membranes which regulate the sense of touch and other perceptive operations in the body as in [Hamill and McBride 95]. Dither for assembly tasks then appears quite natural.

1.5 Organization of Thesis

This thesis forms the beginning steps towards the development of a robust robotic assembly control system. Chapter 2 reviews the literature and current work within related fields. Chapter 3 outlines the kinematic structure and models for this work, illustrates the task coordinates, and states the basic assumptions of the algorithm. Friction suppression techniques are developed from physical models and verified in Chapter 4. Chapter 5 presents a foundation and preliminary investigation for a new force feedback method. Chapter 6 summarizes the advantages and initial success of active force sensing, and Chapter 7 looks ahead to future work and applications of this technique.

Chapter 2

LITERATURE REVIEW

Much study has been performed on dither, friction, robotic control, and surface following techniques. Previous work serves as both a foundation from which to work and a basis for comparison.

2.1 Dither

An initial reference to dither is found in a 1959 issue of *Science* magazine [Weaver 59] in which high frequency vibrating parts serve as a tool for reduction of friction in jet aircraft positioning devices. Similar high frequency vibrations are employed by [Boothroyd, Poli, and Murch 82] in automatic assembly processes. They utilized the vibration for friction suppression, and tuned the frequency and vibration angle so that when coupled with the mean conveyor speed the coefficient of friction was minimized. Tuning of vibrators was also implemented for vibratory work tables to reduce friction between mating parts in [Asada and Li 92]. In this work, position and force feedback parameters were optimized by the Taguchi method. In a related applications, hydraulic actuators commonly employ a fluctuation in the flow, or flexible walls, [Carpender, et. al. 91], to reduce the surface drag. Initial work in the use of dither for one dimensional trajectory correction can be found in [Lee and Asada 94].

The field of tactile sensing has grown rapidly recently. [Russell 90] explains how the sense of touch in humans involves small vibrations in the sensory cells. Disruptions in those vibrations are detected and interpreted by these cells. In fact, the touch senses are poor detectors of absolute quantities, yet are very receptive to changes. Differences in the function of nerve cells are characterized by the frequency at which they vibrate as a measure of the dynamic range they can detect. Similarly [Hamill and McBride 95] in *American Scientist* demonstrate many physiological processes from touch to osmosis which rely on micro-detection and generation in membranes of cells.

2.2 Friction

A wonderful and concise presentation of the physics and modeling of friction can be found in [Armstrong-Helouvry 91]. Presented in the context of machines with lubrication, the principles and basic formulations hold for friction in general. Specifically, careful attention is paid to the dynamic effects of friction within several velocity ranges. A friction model of similar form was employed by [Johnson and Lorenz 91] for precision controlled machines. The objective of their work was the training and on-line adaptation of a feedforward friction compensator. For their particular dynamic system they were able to identify friction parameters, behavior, and sources, and then train an extremely accurate control system. They draw particular attention to low velocity friction effects and the complications due to nonlinear behavior. A tension was detected between the function of integral control and the effects of stick/slip. A dynamic approach was also taken by [Wang, Kumar, and Abel 92]. A simple Coulomb model for friction was used and added to the dynamic equations as a force constraint in the tangential direction. In this way multiple frictional contacts could be accounted for within one term without needing to identify each individually.

[Townsend and Salisbury] 's studies on the effect of friction on sensor signals identifies relationships between the robot dynamic and kinematic properties, and the behavior of force sensor signals with and without stick/slip present. Their most important result was the identification of a limit cycle within the signal in the presense of the nonlinearities caused by the stick/slip. The amplitude and frequency of this limit cycle for their system was found to be a direct function of the system kinematic parameters. Initial formulations for the friction suppression included in this work is found in [Ipri and Asada 95].

2.3 Control Techniques for Robotic Assembly

For as many existing types of robots and robotic applications, there are robot controller designs. Of particular importance here is the work on hybrid position/force control, incorporation of human heuristics, and assembly in uncertain environments. A useful overall reference for robot dynamics and control system can be found in *Robot Analysis and Control* by [Asada and Slotine 86].

Initial discussion on the coordination of position and force feedback information can be found in [Whitney 77]. Corrections in the nominal trajectories of the robot motion were generated individually by position and force feedback loops. Stability guidelines were developed which determined a proportional relationship between the allowable feedback gain and environmental compliance. [Raibert and Craig 81] present the development of the hybrid position/force controller. Coordinated control is especially useful for tasks in which robot degrees of freedom can be divided into those which require force monitoring and those which require position control. Using a coordinate selection matrix, separate control commands are generated for each of the two subset motion spaces, combined, and sent to the robot actuators. A strict requirement is placed on exact knowledge of the interaction stiffness of the operation. [Yoshikawa 93] overcomes this requirement by rederiving the hybrid control laws in terms of a generalized velocity vector. This generalized velocity is more easily estimated and allows for control along unknown surfaces.

Errors introduced to the task environment likewise receive much attention in the literature. As passive corrective techniques such as the RCC hand, [Whitney 82], are limited by geometric constraints, the controls community is responding with active control correction techniques. [Peshkin 90] develops a programmed compliance matrix for uncertain environments which ensures that errors will remain bounded and the system stable. [Yang 95] introduces a progressive learning approach which learns dynamic parameters one by one through specific control input scheduling. Impacts also introduce unexpected errors into a dynamic system. [Youcef-Toumi and Gutz 89] modeled the dynamics of impacts between rigid bodies, and investigated a compensation control law to reduce the effects on the system dynamics. From a mathematical disturbance perspective, [Oldenburger and Boyer 62] analyzed the required relationships between high frequency signals added to nonlinear systems and the regular command signal to assure stability.

2.4 Task Planning and Surface Tracking

Peg-in-hole insertion tasks have been utilized as typical example operations for task planning programs. [McCarragher] uses petri nets to catagorize all possible contact states that may occur during an insertion. Nets are developed for all possible state transitions and then used as guides for adjusting the robot motion commands. The relative merits of passive versus active sensing for such tasks can be found in [Xu and Paul 90].

Algorithms for following unknown surfaces have taken several forms. [Demey and DeSchutter] tracked unknown surfaces using a combination of model-based programming and sensor-based execution. They divided the 'world' into several possible geometric models, and used normal force measurements to define the surface trajectory. They ignored all friction effects, and were limited by their chosen geometric templates. A more computationally intensive off-line algorithm is presented by [Bay and Hemami 90]. From recorded force and position data from each trial, a Kalman filter is continually applied to optimize the end-point position with respect to the surface normal, assuming no friction. The contact models and tracking algorithms of Chapter 5 were first introduced in [Ipri and Asada 94]. An interesting modeling approach for incorporating human heuristics into the generation of robot control commands is presented by [Takahashi, Ogata, and Muto 93]. Tasks were quantified into mini-tasks, described by motion sequences, and then jointed to complete the overall task.

Chapter 3

MODELING

All dynamic analysis associated with this work is performed in the context of a robotic assembly process in which a single point contact exists between the robot end effector and the task environment. The process goal involves a manipulation of the contact, as shown in Figure 3.1. This chapter defines the subset of systems for which the work of this thesis is applicable. Section 1 begins with a determination of the task coordinate systems, followed by the simple dynamic model and assumptions which carry through the work. Section 2 explores the hybrid position/force controller required for successful implementation.

3.1 Physical System

The system can be represented by the dynamic model of Figure 3.2. An estimated interaction stiffness between the end effector and the environment, k_e, accounts for the stiffness of the force sensor and the part contact. Damping in the tangential direction, b_e, represents the friction forces, while in the normal direction damping effects are assumed to be negligible compared to the stiffness. The robot is represented as a dynamic black box between the control input and resulting joint motion. For the purposes of the end effector dynamics, only the actual robot motion needs to be taken into account. The frequency response of each joint is also necessary for control as the robot response to control signals will be based on this information. The dither signals must be chosen such that their possible attenuation does not render the amplitude negligible and the resulting effect on friction is still useful. For friction suppression, the phase shift is not important, whereas for the surface tracking, phase shifts must be measured and accounted for. A relatively high bandwidth force sensor will not interfere with the dither operations.

Three difference coordinate systems are employed for ease of trajectory generation and force sensor interpretation. Each coordinate system is shown on Figure 3.3 The inertial reference frame XY is defined with respect to the home position of the robot (joint angles equal to zero) with positive rotation defined clockwise from the X axis to the Y axis. The endpoint coordinates, x_e, y_e, are measured with respect to the position of the robot end point. x_e points positively out along the line of the second joint arm, while positive y_e is set such that in the robot home position y_e is parallel

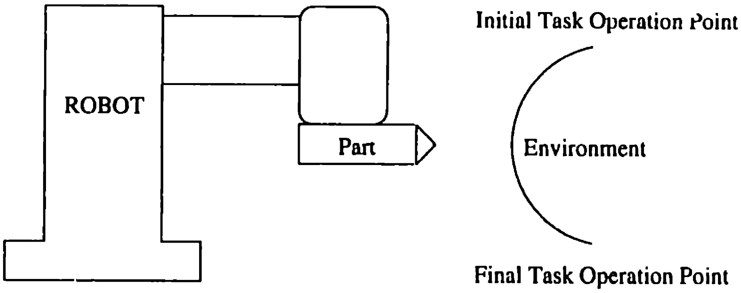
ROBOT
Part
Initial Task Operation Point
Environment
Final Task Operation Point

Figure 3.1: Typical Assembly Task

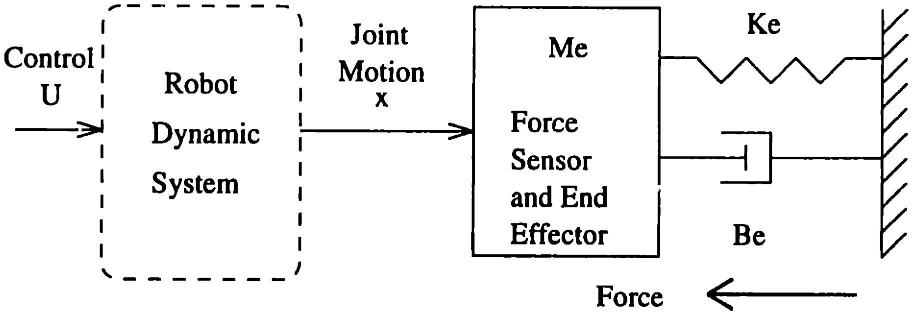
Control
U
Robot
Dynamic
System
Joint
Motion
x
Me
Force
Sensor
and End
Effector
Ke
Be
Force

Figure 3.2: Dynamic System Model

to Y. The task coordinates, xy, are defined with respect to the point of contact. The positive x direction points into the environment always parallel to the surface normal. The y direction lies along the tangent, with positive orientation measured such that $+y$ is parallel to $+y_e$ when $+x$ is parallel to $+x_e$. The robot trajectory is generated in the inertial reference frame, the force sensor readings correspond to end-point coordinates, and identification of friction and the surface properties are defined in the task coordinates.

3.2 Hybrid Control

Performing assembly tasks with the smallest possible contact force to still maintain both contact and control allows for the use of minimal control effort and prevents possible damage to the assembly parts from large contact forces. In order to maintain these low contact forces, a mechanism for force control must be incorporated into the system. For the systems assumed in this thesis, i.e motion is to be controlled along

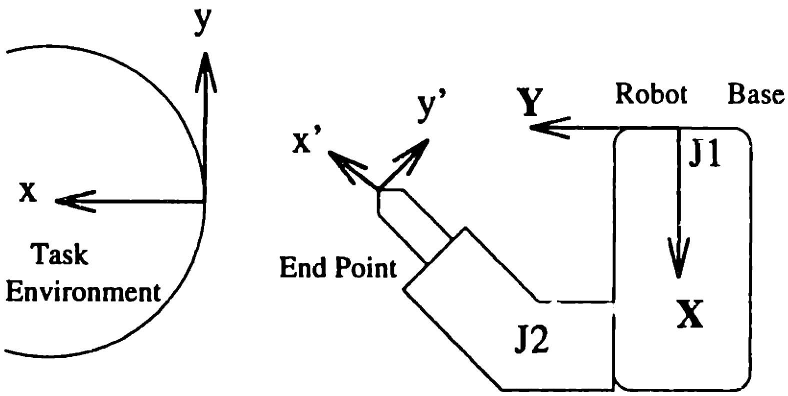

Figure 3.3: Coordinate Reference Frames

the tangential direction and force along the normal direction, hybrid position/force control adequately satisfies both requirements.

Simultaneous position and force control was introduced by [Raibert and Craig 81] as hybrid position/force control. Hybrid control divides the robot degrees of freedom into those for which position is controlled and those which force is controlled. Separate control algorithms use respective feedback commands to generate independent control signals. Those two signals are then combined to produce one control signal sent to the robot. Here a simplified algorithm, shown in block diagram in Figure 3.4, is employed which uses respective force and position feedback signals to generate independent position update vectors. These two vectors are then combined and sent through the inverse kinematics and PID controller to produce one control signal. The control structure is conducted in the task coordinates such that force control occurs along the x direction and position control along the y direction. Generalizing a single position command minimizes the errors of the inverse kinematics and allows for independent force regulation without interfering with the position control algorithm. The matrix R in Figure 3.4 likewise indicates the relevant selection matrix for this system.

Determination of the interaction stiffness is a key component of the hybrid control method. [Raibert and Craig 81] assumed that this stiffness is exactly known. For assembly tasks, this value can be estimated, but will slightly vary with exact normal force and assembly configuration. This stiffness also acts as the force feedback gain. According to [Asada and Slotine 86], if the stiffness is overestimated, the potential exists for driving the system unstable. Underestimating this value will produce a sluggish controller, but will maintain stability. The stiffness of the force sensor is usually extremely stiff, much larger than the contact stiffness, and therefore cannot be used as a limiting value. However, once an appropriate level is achieved either through trial and error or specific measurement, the controller does maintain the force adequately.

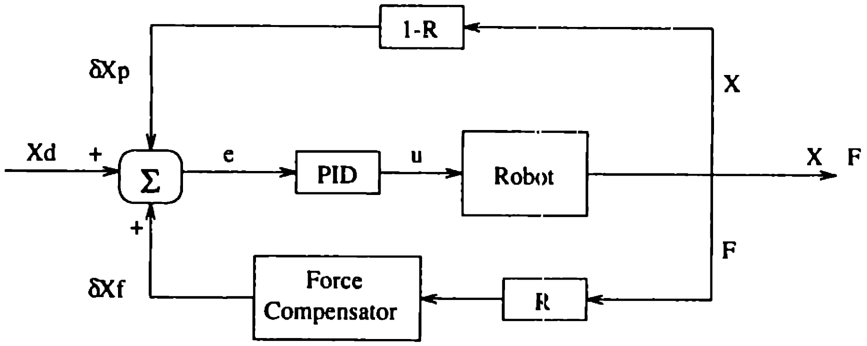

Figure 3.4: Hybrid Position/Force Control

The unique aspects of the control system will be developed in the course of later sections. In general, the position is regulated by a traditional PID controller. The trajectory is generated on-line at each time step based on a nominal trajectory and the corrections for friction and surface topography. The force controller uses an estimate of the interaction stiffness combined with Hooke's Law to determine the trajectory update.

Chapter 4

FRICTION SUPPRESSION

Kinematic friction will be present whenever two surfaces are in contact in relative motion. Although this effect is useful in some situations, such as allowing a person to walk without sliding across the floor, during force-guided robotic assembly friction forces act as disturbances to feedback signals adding unwanted noise to the dynamic system. Entirely eliminating friction, especially in an uncertain environment, is nearly impossible. Yet through a clear understanding of the physics involved, significant success can be achieved in actively minimizing the effect.

4.1 The Basis for Friction Suppression

Many attempts have been made to mathematically model and predict friction forces directly from the relative velocity. Such a model is presented in Section 4.2 and forms a basis for this study. A central result of this model is that because the frictional coefficients are extremely sensitive to the actual contact conditions, prediction of the friction forces will not be precise in uncertain environments. Therefore, any friction model must contribute to appropriate control mechanisms which compensate for these uncertainties.

It has been common practice to maintain a relative motion between objects in contact in order to prevent static friction forces, which are usually higher than dynamic friction. For example, vibratory part feeders keep objects in constant motion to allow them to more easily move between conveyors, as in [Boothroyd, Poli, and Murch 82]. This same concept is now applied to robotic assembly by adding a high-frequency, low amplitude sinusoidal signal to the nominal end-point motion, as discussed in Section 4.3. Whereby, at the point of contact of the two surfaces, the parts remain in constant relative motion. The individual dither effect is significant for reducing the friction, and preventing stick/slip because the velocity changes never initiate from a rest position. Section 4.4 derives a tuning algorithm for the dither parameters by determining their relationship to the resulting force signals. This approach is experimentally verified in Section 4.5.

4.2 Friction Model

To effectively derive a friction suppression algorithm, a physically realistic mathematical description of friction is required. Friction phenomena result from the relative motion of two bodies in contact. The molecular interactions at the contact impose a springlike, static resistance to any low velocity motion or motion initiation. Stick/slip occurs at low velocities when the applied force in the direction of motion is not large enough to overcome static friction. As the robot attempts to move forward, the compliance of the interaction resists the motion and exerts a force which grows as the robot arm continues to move. When this increasing force reaches the static friction level, the end point finally moves relative to the environment, but the interaction force drops back to the applied force level. If this applied force is still lower than the static friction, the end point will stick again and the cycle repeats. If the applied force due to the torque from the robot joint is greater than the static friction level, stick/slip will not occur. The existence of stick/slip is therefore dependent on the interface compliance in the direction of motion. At relatively high velocities, stick/slip will not occur, and a different friction model dominates. Therefore, a functional description must accurately relate the behavior of friction under different velocity regimes.

[Armstrong-Helouvry 91] presents a fairly complete analysis of the various forms of friction encountered in assembly operations. Although his analysis models machine friction, the relationships derived are based on appropriate and accurate physical models, and are generally applicable. Four physically distinct effects of friction which need to be considered are static friction, kinetic friction, Stribeck friction, and velocity dependent friction, shown individually in Figure 4.1. Stick/slip effects, as described, are dictated by a combination of static and velocity dependent friction. Static friction is the "force necessary to initiate motion from rest" [Armstrong-Helouvry 91], usually related to endpoint displacement by a form of Hooke's Law with a characteristic stiffness. Static friction dominates behavior from initial motion and very low velocities until relative motion is achieved. Static friction is presented here for completeness, but will not be discussed further.

$$F_{static} = k_{fric}\Delta x \tag{4.1}$$

Kinetic friction is a component independent of the magnitude of velocity, yet dependent on its direction; represented as

$$F_{kinetic} = F_t sgn(\dot{x}) \tag{4.2}$$

where $sgn(y)$ represents the sign, $(+1, 0, -1)$, of the variable y and $\dot{x}$ denotes the relative velocity at the point of contact. Kinetic friction is commonly represented as Coulomb friction, or by the equation $F_f = -\mu F_N sgn(\dot{x})$, where μ represents the coefficient of sliding friction, and F_N represents the normal reaction force from the environment. This elementary relationship correctly captures the dependence of F_t on the surface characteristics and normal contact force. Rougher surfaces will exhibit a higher coefficient of sliding friction, μ, and hence a higher kinetic friction force. Also, as friction acts as a resistance to motion, the higher the normal force, the higher the

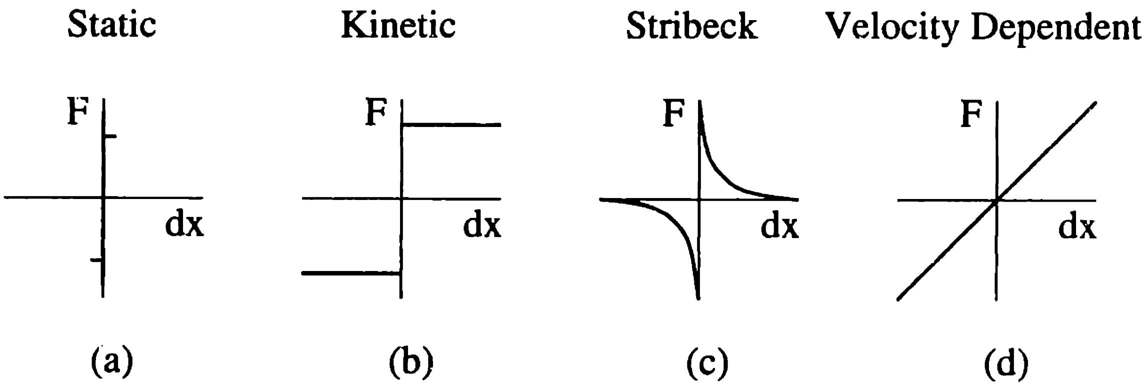

Figure 4.1: Individual Friction Components

friction coefficient. As will be shown, the friction force varies directly with F_N. For this reason, the normal force will be maintained at a constant value throughout the operation. Kinetic friction becomes most pronounced at higher velocities, above the static/sliding transition point.

The Stribeck friction describes the nonlinear friction effects observed at low velocities. In the velocity region just after stick/slip occurs, friction forces begin to decrease as the velocity increases according to a power law, as seen in Figure 4.1(c). A characteristic velocity, $\dot{x}_s$, defines the inflection point for the function. This effect is symmetric about $\dot{x} = 0$, and hence includes a $sgn(\dot{x})$ term. Gaussian exponential and Lorentz forms have been found to best model these effects at lower velocities, [Armstrong-Helouvry 91]. Stribeck friction is therefore taken as

$$F_{stribeck} = \frac{F_s sgn(\dot{x})}{1 + \left(\frac{\dot{x}}{\dot{x}_s}\right)^2} \tag{4.3}$$

The value for $\dot{x}_s$ is a function of the surface roughness and susceptibleness to stick/slip effects. The coefficient F_s acts as a scaling parameter which is related to contact area and surface conditions. Additionally, a component directly proportional to the velocity, a direct damping term due to shear forces, is added of the form

$$F_{velocity} = F_v \dot{x} \tag{4.4}$$

for $F_t, F_v, F_s, \dot{x}_s$ unknown frictional coefficients. The total kinetic plus velocity dependent friction is then

$$F_f(\dot{x}) = F_t sgn(\dot{x}) + F_v \dot{x} + \frac{F_s sgn(\dot{x})}{1 + \left(\frac{\dot{x}}{\dot{x}_s}\right)^2} \tag{4.5}$$

This complete function takes the form shown in Figure 4.2. Note that in this section the friction force is taken to be positive in the direction opposite from the relative velocity of the two surfaces. The minimum point observed in the figure results at

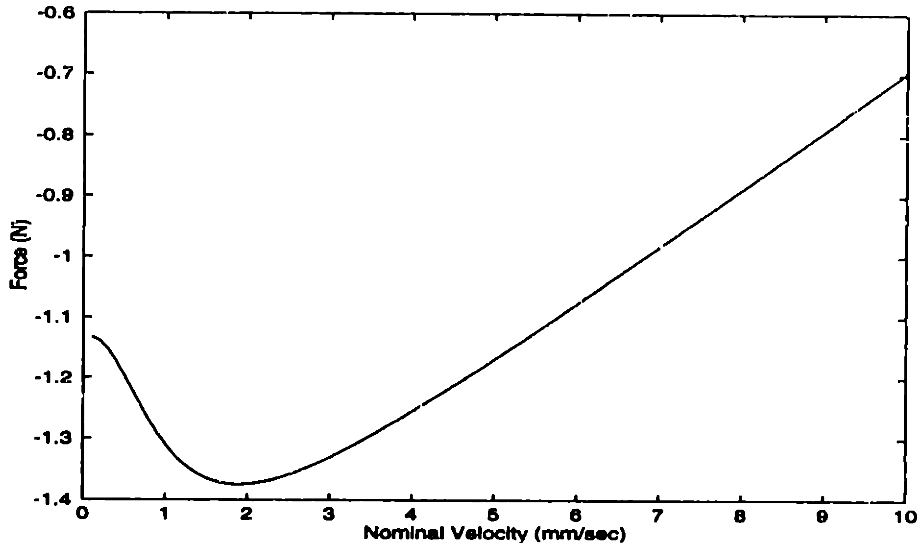

Figure 4.2: General Form of the Friction/Velocity Curve

the point in which the dominating effect changes from Stribeck friction to velocity dependent friction. At low velocities the effect is highly nonlinear, while at higher velocities the friction effects are nearly linear. For the purpose of calculational ease, in some of the following calculations, the Stribeck term is replaced by the power series,

$$F_s sgn\left(\dot{x}\right)\frac{1}{1+\left(\frac{\dot{x}}{\dot{x}_s}\right)^2} = F'_s - F_s\left(\frac{\dot{x}}{\dot{x}_s}\right)^2 \tag{4.6}$$

From the definitions of $F_t, F_v, F_s, \dot{x}_s$, the exact form and value of the friction forces is extremely dependent on the environmental and contact conditions. The normal contact force, surface roughness, contact area, and interaction stiffness and damping all influence the value of this force at any instant. Because of this great condition dependence, the exact friction parameters can only be estimated in the presence of varying or uncertain conditions.

4.3 The Effect of Dither on Friction Forces

This friction model can now be evaluated for the dither operation. Figure 4.3 shows equation 4.5 evaluated for the dither operation in which

$$\begin{aligned} \dot{x} &= A\omega\cos\omega t && (4.7) \\ F_f &= F_t sgn(A\omega\cos(\omega t)) + F'_v A\omega\cos(\omega t) + \frac{F_s sgn(A\omega\cos(\omega t))}{1+\left(\frac{A\omega\cos(\omega t)}{\dot{x}_s}\right)^2} && (4.8) \end{aligned}$$

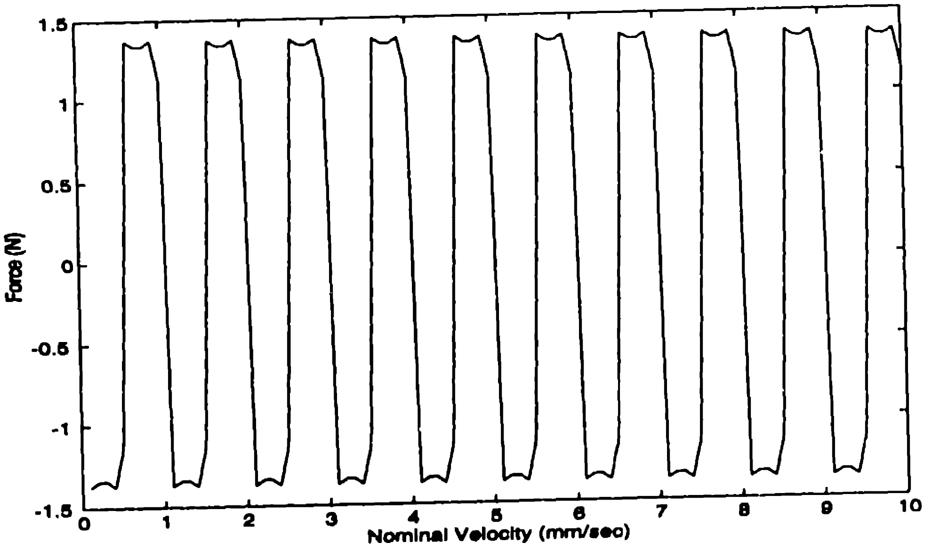

Figure 4.3: Friction Force for Periodic Dither Signal

$$\bar{F}_f = 0 \tag{4.9}$$

Notice that Figure 4.3 illustrates a time history for the force signal. The friction force likewise becomes periodic with the general form of Figure 4.2 repeated at the crests and troughs of each signal. The period frequency is equal to the dither frequency, and the average force value is zero due to the symmetry of the function and the $sgn(\dot{x})$ terms. The amplitude of the oscillations is directly proportional to the dither amplitude, $A\omega$.

When the dither signal is superimposed over a nominal constant velocity, $\dot{x}_o$, the end point velocity becomes:

$$\dot{x} = \dot{x}_o + A\omega\cos(\omega t) \tag{4.10}$$

for which

$$\bar{F}_f = F_t + F_v(\dot{x}_o + A\omega) + F_s - F_s\left(\frac{\dot{x}_o^2}{\dot{x}_s^2} + \frac{(A\omega)^2}{\dot{x}_s^2}\right) \tag{4.11}$$

Figure 4.4 shows the resulting friction plotted against the nominal velocity for a given $A\omega$. The average force value is a function of only the product $A\omega$, not the two variables independently. This term exists throughout the analysis and serves as a characteristic velocity for the dither. Oscillations as in Figure 4.4 dominate the response when the nominal velocity is less than the value $A\omega$. Once $\dot{x}_o$ becomes larger than $A\omega$, the linear, high velocity friction effect dominates with the dither causing a fluctuation to remain in the response level. In the region about $\dot{x}_o = A\omega$, a transition between the two extreme responses is observed. The average force, equation 4.11, is

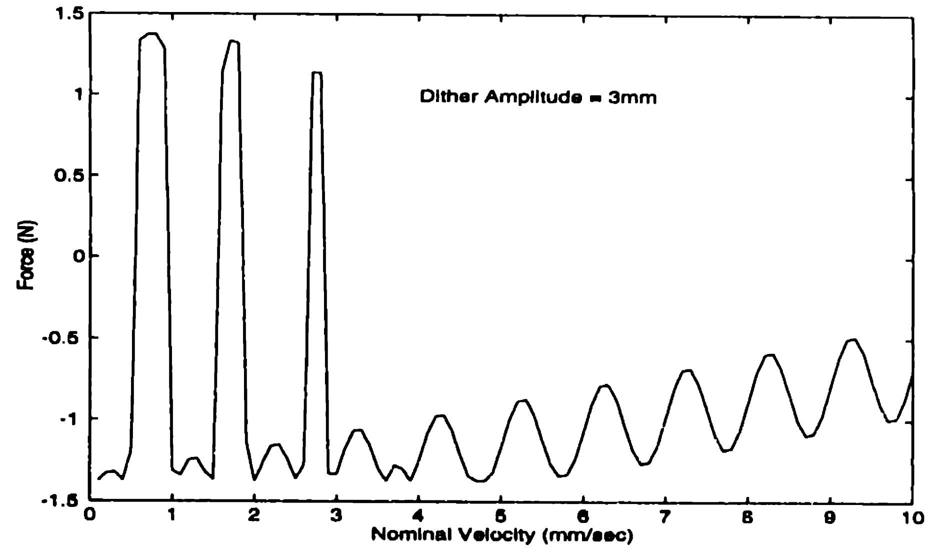

Figure 4.4: Friction Force for a Nominal Velocity and Dither Operation

no longer zero as with the dither alone, and has been reduced by a factor of $\frac{F_s(A\omega)^2}{2\dot{x}_o}$ because of the dither. Figures 4.2 through 4.4 were generated as examples from actual friction coefficients estimated during experimentation.

Therefore, for a dither signal superimposed on a nominal velocity, the expected form of the friction force signal is a low amplitude, high frequency oscillation about an average value. The frequency matches that of the dither, and the average force is determined by the friction force at the nominal velocity without the dither. It has been assumed that during robot assembly tasks, $\dot{x}_o$ is greater than $A\omega$. If $\dot{x}_o$ and $A\omega$ are similar in magnitude, the robot motion would be very jarred. At the greatest value of the dither, the effective robot velocity would be twice that of the nominal velocity, while at the most negative value of the dither, the effective robot velocity is zero. This creates high accelerations and jumpy motion, from which the inertial effects act against the friction suppression.

For the situation in which $A\omega > \dot{x}_o$, the robot appears to be dithering in place with an extremely slow progression. In this case, the friction suppression is excellent as the oscillatory behavior from the dither dominates the response and the average force value is nearly zero. Friction suppression using dither is therefore quite useful for applications in which the nominal velocity and reasonable operating range of $A\omega$ are very different. If these values are similar, the resulting dynamics work against the friction suppression and appropriate adjustments to the dither need to be made.

This behavior strictly demonstrates the effect of varying velocity assuming all other task conditions remain the same. As experimentation and theory shows, other variations such as in the normal contact force will likewise cause changes in the frictional force. The exact phase of the dither signal with respect to the sampling time does not influence the dynamics as the effectiveness of the dither is related to the time integral over one dither period.

4.4 Dither Tuning

Ideally, one would like to produce as minimal a friction force as possible, given a prescribed environment and nominal velocity. Just as the friction coefficients are related to the surface roughness and normal contact force, the resulting friction with the dither operation should also be related to the frequency and amplitude of the dither. Quantifying this relationship will allow for the development of an on-line tuning algorithm to adapt the dither parameters to the resulting friction forces. As discussed, the friction force signal is characterized by oscillations about an average value. The goal of friction suppression then is to minimize both the signal average and standard deviation. Unfortunately, as the oscillation are a direct result of the presence of the dither, they can not be eliminated without eliminating the dither. It follows then, that concentration of effort lies in minimizing the average force value.

With a prescribed environment, and hence a prescribed roughness and interaction stiffness, and a preset nominal velocity, only two adjustable factors remain; namely the normal contact force and the dither parameters. Through use of the hybrid controller, the contact force can be maintained to as small a value as possible which still allows for continual contact of the part and the environment. As mentioned in Section 4.2, the friction coefficients are highly dependent on the normal force and directly affect the friction force for a given $\dot{x}_o$. Any remaining minimizations must result from on-line tuning of the dither parameters.

4.4.1 Existence of An Optimal Parameter Set

Dither tuning starts with the complete friction model,

$$
\begin{aligned}
F_f &= F_t sgn(\dot{x}) + F_v(\dot{x}_o + A\omega\cos(\omega t)) + \frac{F_s sgn(\dot{x})}{1 + \left[\frac{\dot{x}_o + A\omega\cos(\omega t)}{\dot{x}_s}\right]^2} && (4.12)\\
F_f &\approx F_t sgn(\dot{x}) + F_v(\dot{x}_o + A\omega\cos(\omega t)) + F_s sgn(\dot{x}) - F_s sgn(\dot{x})\left(\frac{\dot{x}_o + A\omega}{\dot{x}}\right)^2 && (4.13)\\
\bar{F}_f &= F_t + F_v(\dot{x}_o) + F_s - F_s\left(\frac{\dot{x}_o^2}{\dot{x}_s^2} + \frac{(A\omega)^2}{\dot{x}_s^2}\right) && (4.14)
\end{aligned}
$$

The effect of the dither parameters on the average force value is manifested through the final term of equation 4.14. The average force value can be separated into a constant term and a dither dependent term, herein denoted as

$$\bar{F}_f = \lambda - F_s\frac{(A\omega)^2}{\dot{x}_s^2} \qquad (4.15)$$

As highlighted in the previous section, this term results in a decrease in the average force value. If it is possible for the dither parameters to be set such that this final term has a large effect on the average force from the nominal velocity, a minimal average frictional force can be obtained. Due to the relative magnitudes of the constant term and the dither coefficients, it may be practically impossible to drive this function to zero. The emphasis will therefore be on minimization of this function. In the model equations, the resulting average force value is only a function of the product $A\omega$, not the two variables individually. Therefore, only this characteristic velocity can be tuned by this analysis. As the frequency of the dither mainly affects the oscillation of the output and can be considered as a scaling factor for the amplitude, the frequency will be assumed preset. Choice of this frequency is based on the limitations and bandwidths of the actuators and sensors within the system. An update law, based on the frictional model can now be developed for the dither characteristic velocity.

Minimizing the force value begins with an appropriate cost function,

$$J = \frac{1}{2}F_f^2 \tag{4.16}$$

The actual force value is used in the cost function instead of the average value for mathematical reasons. Use of the average force results merely in a trivial solution. A theoretical minimum value results from the derivative of J with respect to $A\omega$.

$$\frac{\partial J}{\partial A\omega} = \frac{\partial J}{\partial F_f}\frac{\partial F_f}{\partial A\omega} = F_f\left(F_v\cos(\omega t) - \frac{2F_s A\omega\cos^2(\omega t)}{\dot{x}_s^2}\right) \tag{4.17}$$

Setting equation 4.17 to zero, the optimal value of $A\omega$ is found to be

$$(A\omega)_{opt} = \frac{F_v}{F_s}\dot{x}_s^2 \tag{4.18}$$

This result indicates a balance between the kinetic friction term and the Stribeck friction term. Physically and intuitively such a result is extremely logical. As indicated by Figure 4.2, the Stribeck term continually decreases with increasing velocity, setting a minimum point for the optimal value. Coupled with this is a maximum desired limit due to the kinetic term increasing with velocity. The minimum point on the figure is the balance of dominance of the two terms. As inferred above, this is merely a theoretical optimal value for the amplitude and its practicality is dependent on the exact parameter values involved.

4.4.2 Parameter Update Law

For application to robotic assembly tasks in uncertain environments, the power of this friction suppression algorithm will be the ability to continually adjust to varying frictional coefficients. From the cost function of equation 4.16, an update law for the dither characteristic velocity is now developed. Using a gradient decent approach,

$$\Delta(A\omega) = -\eta\frac{\partial J}{\partial(A\omega)} = \frac{\partial J}{\partial F_f}\frac{\partial F_f}{\partial(A\omega)} \tag{4.19}$$

To calculate the partial derivative of F_f with respect to $A\omega$, an average functional value replaces the cosines such that

$$\|\cos\| = \frac{1}{2} \tag{4.20}$$

Then the friction force becomes

$$F_f = \lambda + \frac{F_v A\omega}{2} - \frac{F_s (A\omega)^2}{4\dot{x}_s^2} \tag{4.21}$$

The final update law is then

$$\Delta(A\omega) = -\eta F_f \left(\frac{F_v}{2} - \frac{F_s}{2\dot{x}_s^2}(A\omega) \right) \tag{4.22}$$

which is simply implemented on line.

4.5 Verification and Experimentation

4.5.1 Experimental Set-Up

The dynamic system under study consists of a direct drive planar robot, outfitted with a six axis force sensor placed just prior to the assembly part. The robot second link was specially designed for minimal inertia. The end effector consists of an aluminum pointer for improved observability and minimal contact with the environment. The external part, or environment, is a flat object of known material and geometry, and estimated orientation. The surface contained random, small variations and burrs to simulate an unknown surface with varying friction coefficients. Note also that the terms tangential force and friction force are used interchangeably to indicate the same values depending on the more natural terminology.

The force sensor is a six axis Advanced Technologies Inc, 30lbs/100inlbs (130N/10Nm). limit unit. The stiffness in the normal and tangential directions is $8.8e6 N/m$ and $17e6 Nm/rad$ in the perpendicular torque direction. The contact stiffness will vary with each surface, and for this case is uniformly kept as a metal on metal contact with an stiffness of $10e3 N/m$. For this particular application, the contact stiffness is much less than the force sensor and hence dominates the dynamics. This many not be the case for all applications.

Frequency response tests on each joint indicate a workable bandwidth of 3 Hz for the first joint and 15 Hz for the second. As such the dither operations are divided into two regions. The high frequency motion will be commanded at a frequency above 5 Hz. As long as the attenuation does not render the amplitude negligible, the effect on friction is still useful. For low frequency surface tracking, the dither will occur at a frequency at or below 1 Hz. For this operation, the phase shift is important while the exact frequency is not. The relatively high bandwidth of the force sensor does not interfere with the dither operations.

4.5.2 Experimentation

Experimental verification of the friction suppression algorithm will include

1. Calculation of friction coefficients
2. Demonstration of the friction forces with and without dither
3. Variation of tangential force with normal force
4. Comparison of different dither amplitudes
5. Tuning of dither amplitude

Each of these tasks builds on the others to form the complete friction suppression control structure.

1. Calculation of friction coefficients

   The values for the friction coefficients were evaluated from a series of tests run at varying constant velocities. The values are:

$$\begin{aligned} F_t &= -1.6771 \\ F_v &= 0.0976 \\ F_s &= 0.5400 \\ \dot{x}_s &= 10mm/sec \end{aligned} \tag{4.23}$$

   The dominant term is clearly the kinetic friction coefficient, F_t. Although independent of the velocity magnitude, this parameter will vary with the normal contact force. The velocity dependent coefficient, F_v, is quite negligible in comparison; yet as it will be multiplied by the nominal velocity, it still plays an important role. This value is also related to the shear forces, and will be much greater for rougher surfaces. The characteristic velocity, $\dot{x}_s$, is fairly small, as expected.

2. Demonstration of friction forces with and without dither

   First, the general effectiveness of dither for friction suppression can be realized through the comparison of data collected without dither and data collected with dither of constant parameters. Figure 4.5 shows graphs of two force histories, taken by performing the same task. In the top graph, no dither is applied to the operation. As such, the signal contains fluctuations of random magnitude corresponding to variations in the surface roughness, and no progression towards a zero average force exists. The second graph was recorded with the dither operation added open-loop to the system. The fluctuations observed are regular in magnitude and frequency and the average force value decreases towards zero. Without any feedback control or prior analysis, the effectiveness of dither is still evident.

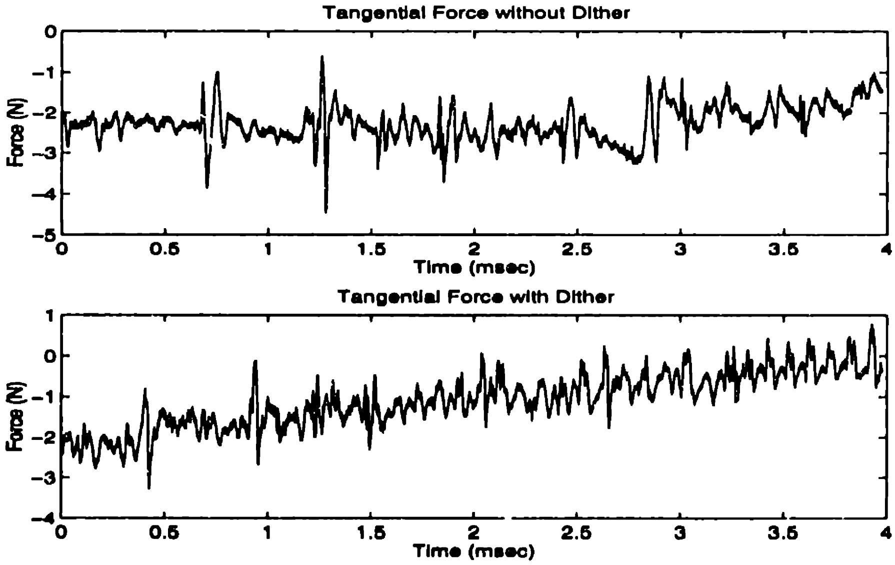

Figure 4.5: Friction Forces with and without Dither

3. Variation of tangential force with normal force

   With use of the hybrid controller, regulation of the average normal force is achieved. Due to the direct dependence of the tangential force on the normal force, the average tangential force likewise is regulated. This effect can be directly observed. Figure 4.6 exhibits the history of both the normal and tangential forces without force control, holding all other control parameters equal. Notice the exact match of changes in average value. The magnitude of the changes is not one-to-one, but are consistently proportional. Likewise, if the contact force is maintained at a constant value, the tangential force maintains its constant average value. Consequently, the force control embedded in the hybrid control scheme provides a convenient means for regulating both the average nominal friction force and a constant baseline for measuring the effects of the dither tuning algorithm.

   From these results, the coefficient of sliding friction, approximately equal to $F_t + F_v\dot{x}$, is estimated to be $0.7N/N$. This value will be used later to adjust for variations in the contact force during the dither parameter tuning. The calculations are shown in Figure 4.6.

4. Comparison of different dither amplitudes

   To illustrate the variation of signal oscillation with different dither amplitudes, the dither amplitude was periodically increased in the course of one trial. Figure 4.7 demonstrates the resulting output. Notice first that the frequency of oscillation remains constant and equal to the dither frequency of $10Hz$. The

	Fn	Ft	Ft/Fn
Trial			
1	1.750	1.179	0.674
2	2.015	1.462	0.725
3	2.156	1.425	0.661
4	2.645	1.840	0.696
5	3.886	2.813	0.724
6	5.263	4.084	0.776
	Coefficient of Friction=		0.709

Figure 4.6: Variation of Tangential Force with Normal Force and Determination of μ

change in amplitude did however have a significant impact on the oscillation magnitude which doubles with a $5mm$ increase in amplitude. This trial was run at a low nominal velocity compared to the dither characteristic velocity, and the tangential force shown is normalized about zero. The growth in the signal standard deviation follows directly from the increases in the dither amplitude. In actual tasks, this effect is combined with the influence of the normal force and the ratio of the velocities.

5. Tuning of dither amplitude

As theory and experimentation indicate, the signal oscillation, and hence the signal standard deviation, is a function of the dither parameters and friction coefficients. This function can be found mathematically as

$$\begin{aligned} \sigma_f^2 &= \frac{1}{T}\int_{t-T}^{t}\left(F_f - \bar{F}_f\right)^2 \\ &= \left(\frac{F_v}{4} + \frac{F_s}{2\dot{x}_s^2}\right)(A\omega)^2 + \left(\frac{F_s^2}{4\dot{x}_s^4}\right)(A\omega)^4 \end{aligned} \tag{4.24}$$

Of all the friction coefficients, $\dot{x}_s$ is the most difficult to determine, and hence the most likely to contain a large estimation error. To reduce the effect of this error, equation 4.24 is used to first estimate $\dot{x}_s$ during each time step. Equation 4.24 contains all variables which are known or measureable. The standard deviation follows from the force signal, the dither characteristic velocity is known, and the other

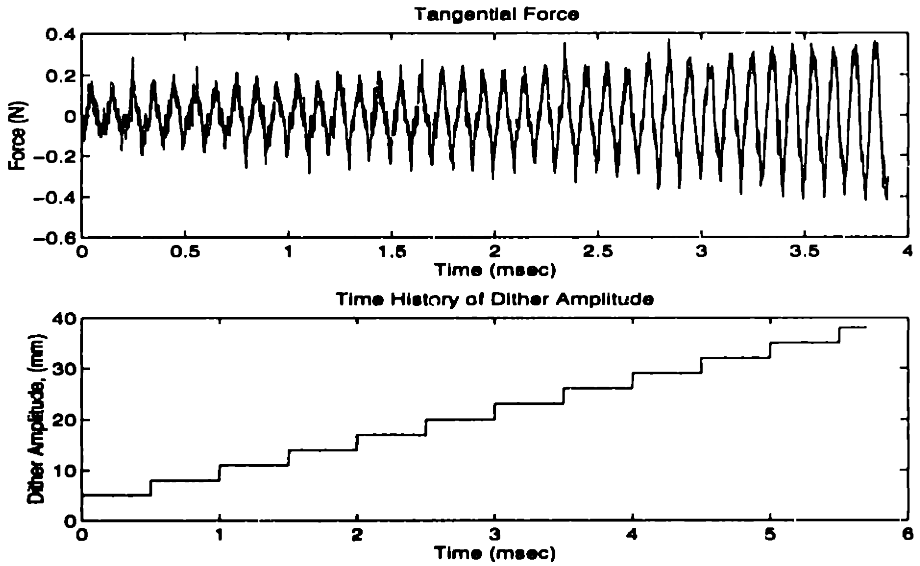

Figure 4.7: Change in Signal Oscillation Magnitude with Dither Amplitude

friction coefficient estimates were previously obtained. This updated $\dot{x}_s$ value is then used for the dither characteristic velocity update law. By continually updating its value based on the exact signal measurements, the update function remains accurate. Experimentally then, the parameter update is performed in two parts.

The results of dither tuning are shown in Figure 4.8, Figure 4.9, and Figure 4.10. The learning rate for the tuning algorithm was kept at a very low value so that the gradual effect of the parameter change could be visualized. Also, the standard deviation of the force signal is measured through a traveling average over the most recent $250msecoftime$. This averaging greatly attenuates the expected response of the dither amplitude to the large spike which occasionally appear in the force signal. Figure 4.8 shows a dramatic rise of the tangential force to zero. This was the largest effect measured. In Figure 4.9, the algorithm brought the dither characteristic velocity to a value such that it become comparable to and then greater than the nominal velocity. Initially the nominal velocity was dominant and a steady nonzero average value existed from $0 - 1.25sec$ During the transition section from $1 - 2sec$, the signal became worse as predicted. Once the dither characteristic velocity overtook the nominal velocity, the average friction force actually did reach a zero value. Figure 4.10 also illustrates the accompanying change in amplitude. Without much variation in the normal force, the rise in the tangential force directly follows from the amplitude rise. The velocities for these tests were specifically chosen such that equivalent nominal and dither characteristic velocities were achievable. Further comments on these results follows in Section 6.1.

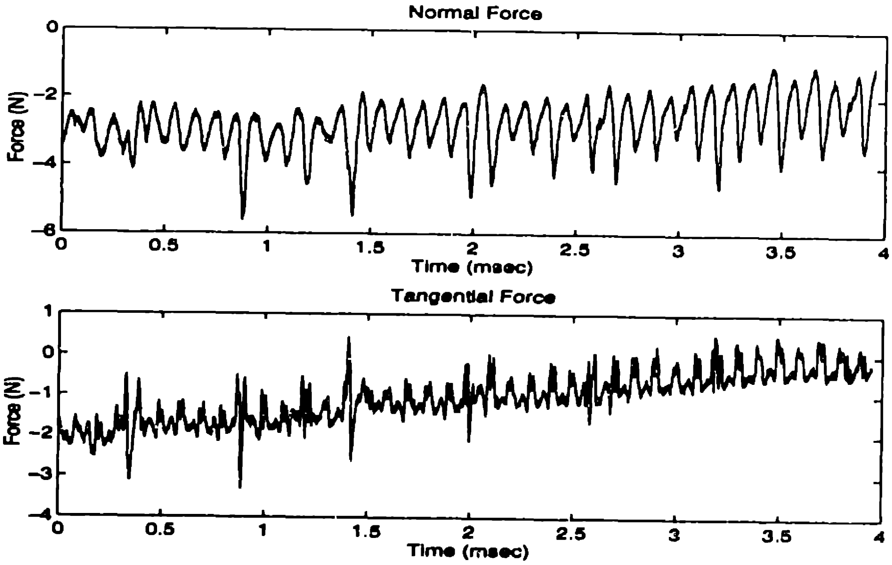

Figure 4.8: Tuning of Dither Amplitude

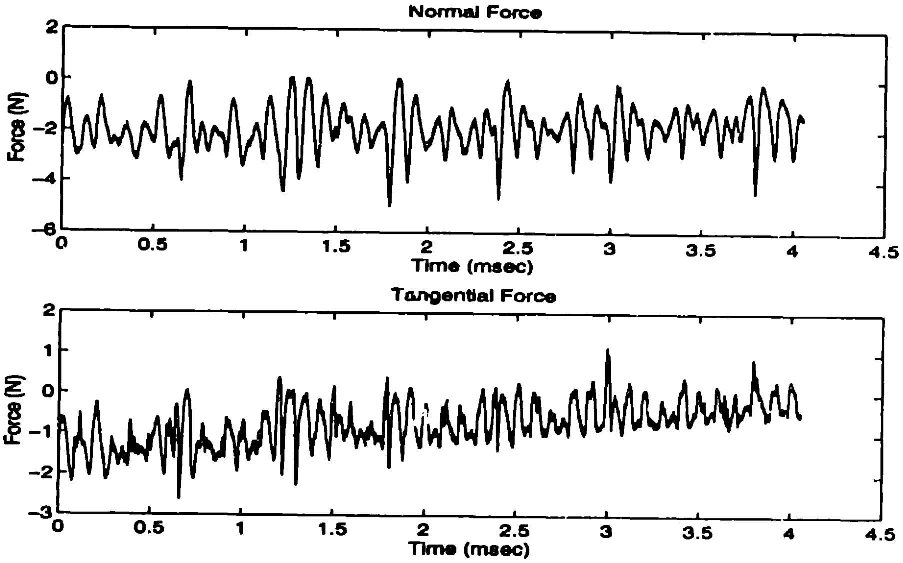

Figure 4.9: Tuning of Dither Amplitude

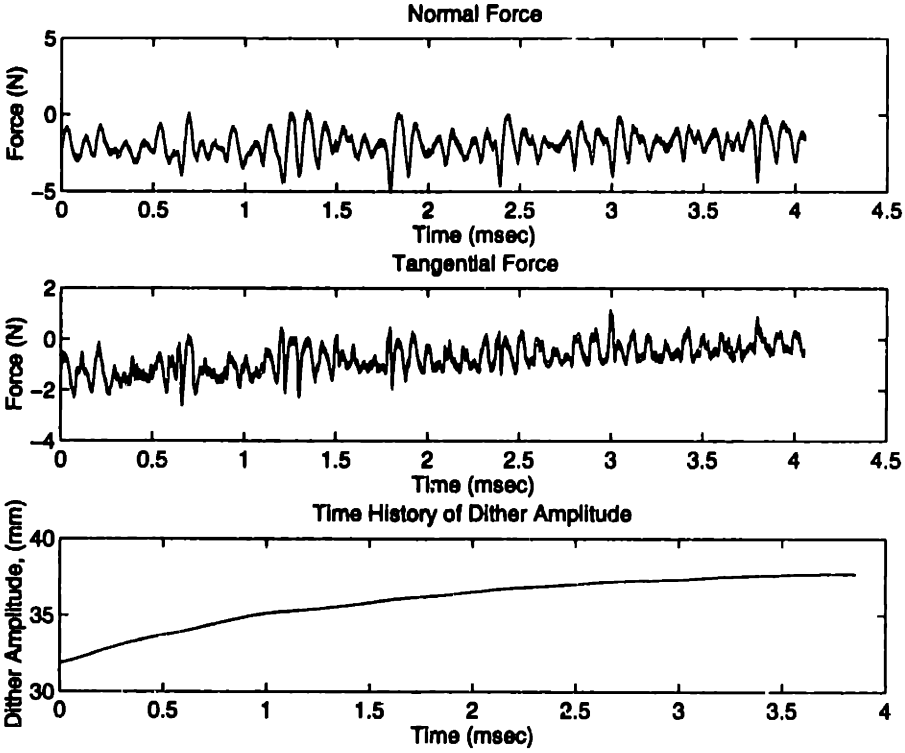

Figure 4.10: Tuning of Dither Amplitude

Chapter 5

SURFACE TRACKING

Surface tracking and detection play a primary role in many assembly tasks, including following an edge for welding and complex part insertions. Although the action may appear complex, surface tracking is simplified by the ability to gain knowledge of the surface through a single variable, the local tangent. This chapter performs a kinematic analysis to relate measured force feedback signals to the unknown tangent. Section 1 discusses the use of force feedback, and Section 2 outlines preliminary studies which help define the task at hand. Section 3 builds a complete model for the case of a single point contact, and that model is combined with a dither operation in Section 4 to complete the surface tracking algorithm. Section 5 concludes with an extension of the algorithm to tasks with multiple contact points.

5.1 Surface Tracking Through Parameter Estimation

Force feedback is a commonly used and effective technique for parameter estimation, and one that is well-suited for assembly control systems. For surface tracking, the key parameter of interest is the surface tangent in the direction of motion. Within the framework developed for friction suppression, differentiation of the normal force versus the tangential force is valuable information for making this distinction as a clear reaction force is expected in the normal direction, and no forces are expected in the tangential direction. This algorithm defines the relationship of the force feedback with respect to the task coordinates such that this differentiation is more easily conducted.

Even though fundamental insertion process also forms an integral part of many assembly systems, it is often the exact source of difficulty for adequate robotic assembly. The novelty of this dither technique is that the kinematic parameters are determined explicitly from measured feedback as the robot trajectory is updated. This surface tracking technique is unique in its determination of admissible and constrained motion space through perturbation of the robot control signals in such a way as to render the calculations independent of uncertain kinematic parameters. The theoretical framework and simulations are presented for the general insertion task, with implementation to occur through later study.

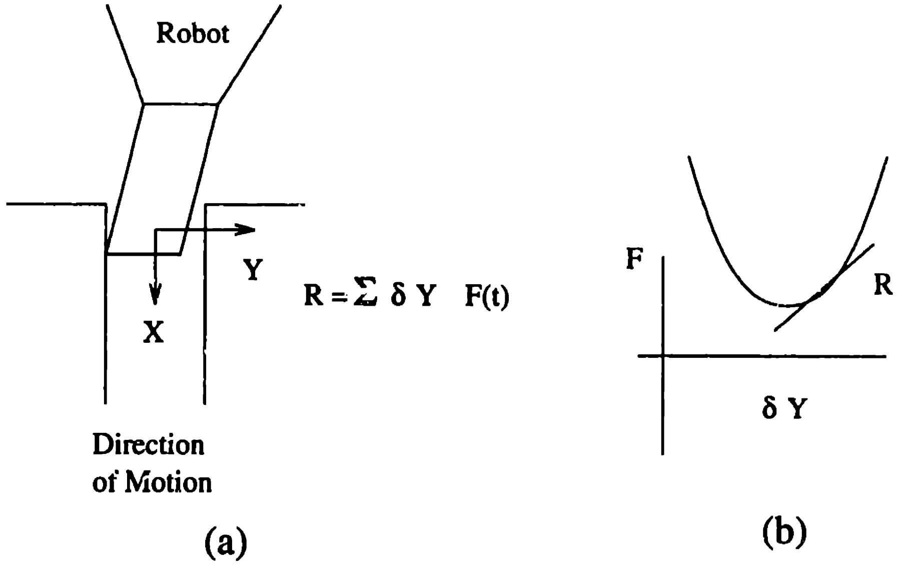

Figure 5.1: Use of Dither for One Dimensional Trajectories

Ideally a surface tracking algorithm would involve the capability for localized accurate detection of parameters without causing too much of a disruption to the overall operation. Likewise, this algorithm must be performable on-line. A minimal number of measurements and calculations as well as minimal dependence on other states is desirable. Use of a localized, small-amplitude dither motion meets these criteria and is easily implemented on-line.

5.2 Preliminary Studies

[Lee and Asada 94] have previously applied dither techniques for determination of one dimensional trajectory adjustments during the insertion of long copper pipes into heat exchange units, as shown in Figure 5.1 (a). The nominal trajectory was a straight line, but due to irregularities in the hole surface, the trajectory had to occasionally be offset by δy in a direction perpendicular to the insertion direction. Determination of δy was performed by adding a dither in the y direction and correlating the force and position measurements. The statistical value of $\frac{\delta F}{\delta y}$ is then proportional to the required trajectory offset, with the optimal position y_o obtained by moving along the curve in Figure 5.1 (b) towards the minimum point.

To determine the applicability of such an algorithm to a two dimensional task, the underlying theory was expanded and then simulated for a surface tracking example. The plant is represented by the function $y = f(x, W)$, where x and y are cartesian coordinates, x is a linear function of time, and W is a vector of coefficients. The control objective is to converge an initial estimate, $\hat{f}$, to the actual function, f, by updating the vector cf weights, W. The quadratic cost function

$$J = \frac{1}{2}[f - f_d]^2 \tag{5.1}$$

is chosen. To minimize J, the update law for W based on a gradient decent algorithm becomes

$$\begin{aligned} \Delta W_i &= -\eta \frac{\partial J}{\partial W_i} \\ &= -\eta \frac{\partial J}{\partial f} \frac{\partial f}{\partial y} \frac{\partial y}{\partial W_i} \end{aligned} \tag{5.2}$$

The first term of equation 5.2 follows directly from equation 5.1

$$\frac{\partial J}{\partial f} = (f - f_d) \tag{5.3}$$

and $\partial y/\partial W_i$ estimated from $\hat{f}$.

A correlation between the forces and dither motion is performed to generate $\frac{\partial f}{\partial y}$ over the sampling points j, and convergence would be realized when $\Delta W_i \to 0$.

$$\frac{\partial f}{\partial y} = \sum_j \frac{(y_{t_j} - \bar{y})(f(t_j) - \bar{f})}{(y_{t_y} - \bar{y})^2} \tag{5.4}$$

Simulations were carried out for a variety of functional forms including quadratic functions and sinusoids. To determine the algorithm's on-line capabilities, the trials performed only iteration for estimating the true function. In the event that the initial conditions were similar to the actual function, the weights converged to their desired values as in Figure 5.2. Success was not as clear for initial conditions outside of the true range. The algorithm also had difficulty detecting and recovering from discrete changes in the surface tangent. The initial estimate of the piecewise function in Figure 5.3 was within 10%. For sinusoidal functions, the algorithm could converge to the proper signal amplitude if the initial frequency was exact, otherwise the system again failed to converge.

This method attempted to create a global map of the trajectory through local adjustments. The largest problem was that errors or very imprecise measurements in the initial estimate were increasingly difficult to compensate for as time progressed. Errors simply multiplied without a mechanism for correction. Errors in the coefficients for high powers of x multiplied exponentially faster than those for lower orders. Likewise, i parameters based on the degree of f had to be estimated in a single operation. As only one dither operation was employed, the entire task space was not explored and hence, the persistent excitation condition was not satisfied. A dither added in the x direction did not increase the algorithm effectiveness, as each update was conducted separately without combining the results of the two dither operations and the persistent excitation condition still was not satisfied. Consequently, an algorithm which held the advantages of the dither, yet always satisfied the persistent

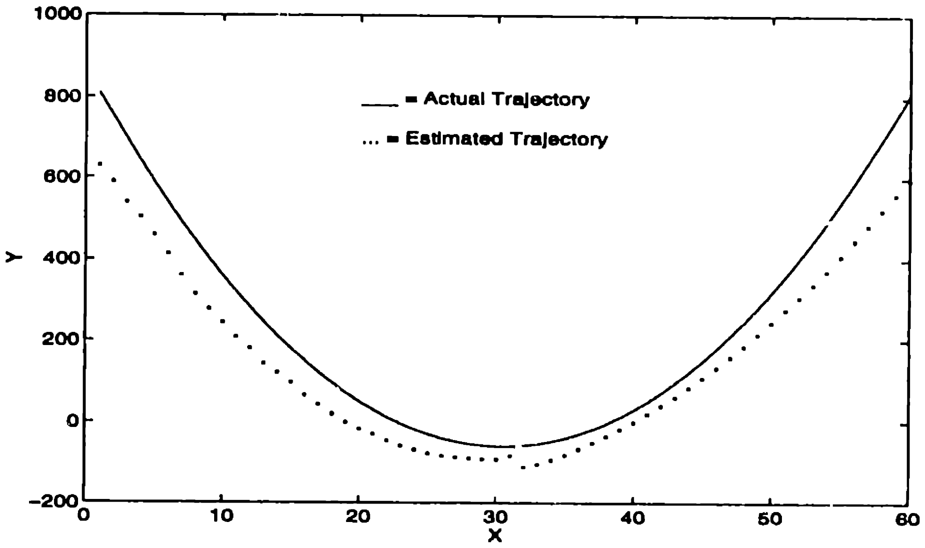

Figure 5.2: Successful Dither Estimation of A Quadratic Function

excitation condition, involved a local versus global calculation, and estimated a minimal number of parameters would prove more accurate.

5.3 Estimation of Surface Tangent Using Dither

In developing an appropriate form for the dither function to estimate the surface tangent, the relationship between the dither operation and the definition of the task space must be known. A distinction is made between the admissible motion space and constraint motion space. The admissible motion space includes the subset of all points within the robot workspace not occupied or blocked by an obstacle. The constraint motion space is the remaining environment, wherever the robot cannot move. In estimating the surface tangent, the boundary between these two spaces is of interest, assuming that the admissible motion space is at least multiply connected. It follows therefore, that in order for the robot to remain in contact with a part in the environment, the robot must operate along the boundary between these two spaces. The distinct properties of this boundary allow for a clearer mathematical definition of the desired robot trajectory. Since the constraint space includes any individual constraints in the system, characterization of the constraint space can be reduced to a single parameter which is defined at the boundary of the constraint and admissible motion space. The desired robot motion should then be defined with respect to this parameter. A simple metric, which easily lends itself to defining trajectories, is the slope of the constraint boundary at any given point. This slope is interpreted as the instantaneous direction of motion for the robot. Therefore, what remains for characterization of the constraint motion space is a method for detecting this slope once contact is made with the obstacle. The dither operation performs this function, working within the bound of a prescribed model. As the dither can act in

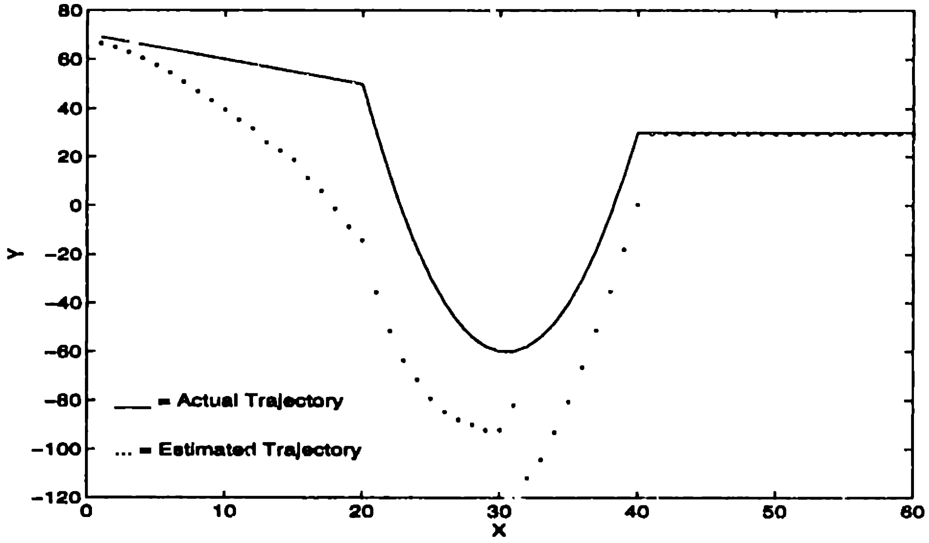

Figure 5.3: Poor Dither Correlation from unknown Initial Conditions and Discrete Changes

the localized region just on the constraint boundary and move in any direction, the persistent excitation condition is satisfied, and estimate of the slope is valid.

5.3.1 Contact Models

A simple model of the dynamic interaction of the robot and the environment for the single point contact case is shown in Figure 5.4. A stiffness k_e is associated with the interaction between the robot and the surface including any stiffness within the force sensor. Throughout the process, the robot is positioned such that an initial penetration into the environment, δy_o, exists. At the point of interaction, a surface tangent t and normal n exist as shown. Initially, only an estimate of these directions, $\hat{t}, \hat{n}$, is known. The angle between the true tangent and the estimated tangent is denoted by α_o. The goal of the surface tracking algorithm in this localized region is to determine α_o.

For planar surface following tasks, the admissible motion space is defined by the tangential direction, while the constrained force is in the direction normal to the surface. Intuitively, without friction, a dot product of the measured forces with the normal direction isolates the static reaction force in the constrained motion space. For equal magnitude displacements, the reaction force from motion in any direction is linearly proportional to the difference between the angle of the surface tangent and the angle of the motion. Motion along the tangent results in no reaction force, while motion in the normal direction will result in the highest force. When a periodic motion occurs, the reaction force following one period will have a sinusoidal form with a variance, or height, proportional to the motion displacement in the normal direction.

Let the measured force reading from the sensor be denoted as F_{f_s}. The reaction

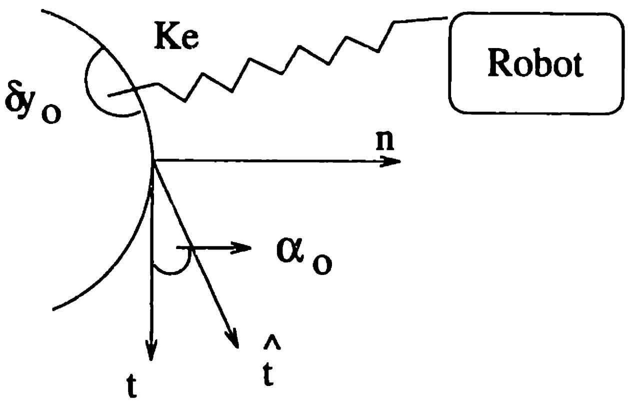

Figure 5.4: Single-Point Contact Model

force in the estimated normal direction is then determined from a projection onto $\hat{n}$ and should be equal to the force according to Hooke's law:

$$F_N = F_{f_s} \cdot \hat{n} \approx k_e \delta y \tag{5.5}$$

5.3.2 Theoretical Model

Given the single-point contact model of section 5.3.1, a more satisfactory method for determination of the surface tangent using dither can now be developed. During the task, the robot is set along a given trajectory in its admissible motion space. Upon detection of contact with the surface, the robot changes course and begins moving along an estimated trajectory, maintaining a constant preload contact force. This trajectory is the preprogrammed motion path in the event that no errors or misalignments have occurred. The hybrid controller maintains a constant normal force while following the trajectory. In maintaining a given distance from the surface, the force controller serves as a first step in ensuring accurate tracking. The adjustments from this controller can account for very small variations in the trajectory, such as minor material imperfections. Yet by the very nature of the hybrid controller, the force compensation occurs only in one direction. In the event that moderate or large unknown changes in the surface tangent occurs, a more direct measurement must be employed.

Detection of a large deviation from the known trajectory is made through a series of limits on the force feedback measurements. If a sudden change in force level occurs, the dither operation is begun. This change could signal loss of contact or attempts to push into the environment. The dither operation consists of stopping the robot and perturbing the contact point in a periodic, defined motion at two known angles. The periodic signal is a sine wave of small amplitude and low frequency. The low frequency reduces the phase shift and allows for accurate joint encoder and force measurements to be collected. The signal is divided into discrete motion steps based on the sensor resolution and actuator bandwidths. The dither angles are set at small

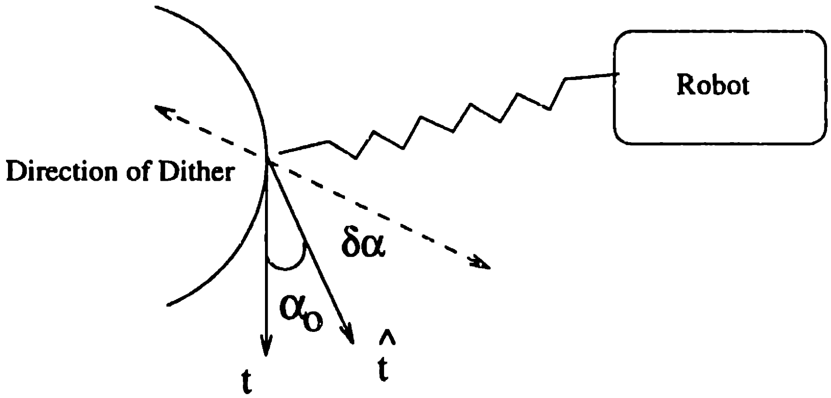

Figure 5.5: Dither Operation in the Task Space

deviations from the estimated tangent, $\delta\alpha_1$ and $\delta\alpha_2$, usually 5^o and 10^o respectively. Implementation of this method is shown in Figure 5.5.

At each step of the dither operation, the resulting reaction force is obtained from force readings. Determination of the tangent begins by calculating the root mean square of $F_N - \bar{F}_N$ over one dither period,

$$\begin{aligned} RMS(F_N - \bar{F}_N) &= \left[\int_0^{2\pi/\omega} (F_N - \bar{F}_N)^2 dt\right]^{1/2} \\ &= \sqrt{\frac{\pi}{\omega}} k_e A \left|\alpha_o + \delta\alpha\right| \end{aligned} \tag{5.6}$$

For $\delta\alpha = \delta\alpha_1$, $RMS = R_1$ and for $\delta\alpha = \delta\alpha_2$, $RMS = R_2$,

$$\begin{aligned} R_1 &= \sqrt{\frac{\pi}{\omega}} k_e A \left|\alpha_o + \delta\alpha_1\right| \\ R_2 &= \sqrt{\frac{\pi}{\omega}} k_e A \left|\alpha_o + \delta\alpha_2\right| \end{aligned} \tag{5.7}$$

Then for $(\alpha_o + \delta\alpha_1)(\alpha_o + \delta\alpha_2) > 0$

$$\alpha_o = \frac{R_1\delta\alpha_2 - R_2\delta\alpha_1}{R_2 - R_1} \tag{5.8}$$

The actual surface angle is therefore a simple function of measured force values and preset angles. Within a small region about the real tangent such that $\alpha_o \ll 1 rad$, and $\delta\alpha_1 = -\delta\alpha_2 = \delta\alpha > 0$,

$$\alpha_o = \frac{R_1 - R_2}{R_1 + R_2}\delta\alpha \tag{5.9}$$

The two dither operations frees this method from relying on the dither amplitude or frequency, the stiffness of the robot interaction, or the friction forces. Without any dependence on the dither parameters, exact tuning of these values is not necessary. As long as the same magnitude and frequency are applied for the two complimentary dither operations, these parameters can be set to match other physical limitations of the particular task, such as the bandwidth of the dither actuator or the force sensor filter frequency.

Choice of dither angles are arbitrary and should chosen based on the physical limitations of the robot and knowledge of the size of parts involved in the assembly operation. Angles closer together provide a better localized estimate of the tangent, yet are limited by the resolution of the actuators. In the event that $R_1 = R_2$, a simple increase in the angle and redithering will provide acceptable information. Such parameters must be optimized for the particular system taking into consideration these limitations.

The angle determination calculation can also take several recursive forms depending on the nature of the remaining controller and the dynamic system. Equation 5.8 easily leads to a recursive formulation in which the recursive least squares algorithm can be applied to solve for α_o. This formulation can be used on-line in regions of constant or slowly varying slope and known kinematic parameters. In the following equation, all variables are known with the exception of α_o, which is to be determined.

$$R = \sqrt{\frac{\pi}{\omega}} k_e A \alpha_o + \sqrt{\frac{\pi}{\omega}} k_e A \delta\alpha \tag{5.10}$$

This alternate formulation was not implemented for this robot tracking task, as the exact kinematic parameters are unknown, and the low bandwidth of the actuators causes great difficulty in controlling the phase lag of the dither signal. In general, choice of formulation depends on the application and source of force measurements.

5.3.3 Simulation

As a proof of concept, this control system was simulated on MATLAB. Random numbers were chosen for initial parameter values. A series of two dimensional trajectories under varying degrees of noise within the system were tried along with sinusoidal functions. Figure 5.6 shows the simulation of tracking a sinusoidal surface. Random gaussian noise was also added, to which the algorithm proved robust. Errors occur around the areas of greatest curvature, as to be expected. This surface is similar to the one the preliminary algorithm failed to estimate. These simulations prove the viability of this technique, but are limited in their ability to predict performance in actual physical systems. For this reason, further testing and results will no be presented until the algorithm can be tested on an actual robot.

5.4 Multiple Point Contact Manipulation

The theory of the previous section can be extended to three degrees of freedom in a straightforward manner. Translational motion components are equivalent to single point contact; therefore, the concentration here is on rotations and insertions. Many

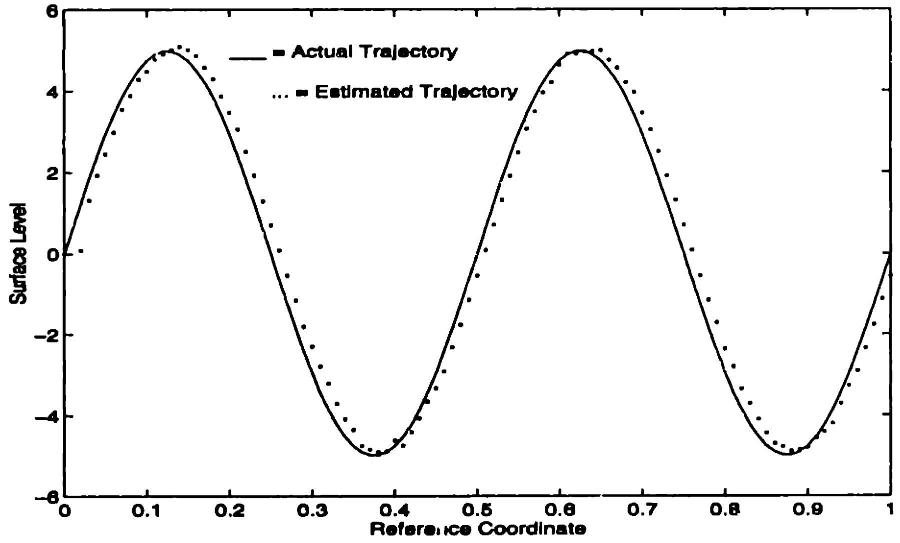

Figure 5.6: Simulation of Surface Tracking for Sinusoidal Function

tasks are more complex than a single point contact, and using the basis set from that model, the extension to multiple contact points is more realistic. No assumption is made with regard to the number of contact points, with the exception that the possibility exists for differentiation of the admissible and constraint motion spaces. Within the scope of this thesis, only the theoretical derivation of the method and simulation results will be presented.

5.4.1 Multiple Point Contact Assembly

In more complex planar assembly tasks the robot has three degrees of freedom, x, y, and θ, and is free to make multiple contacts along any surface of the environment. Contacts along parallel directions act as one point since each of their dynamic effects on the task is the same. The task for the robot is to manipulate the object to a particular alignment. The dynamics for rotational motion can be reduced to the form of the previous section, with the exception that the true instantaneous center of rotation, P, not each of the surface tangents, must be determined. This center rotation lies at the intersection of all the surface normals in which the body is in contact, and hence serves as an indicator of the boundary between admissible and constraint motion space. Admissible motion space consists of rotations about the part's instantaneous center of rotation, or motion away from the environment. Motion into the boundary and hence, rotation about any other point in the part defines the constraint motion space. A process model similar to that for the single contact point state is developed. Figure 5.7 illustrates a body in a plane with x, y, and θ degrees of freedom.

Associated with each coordinate is a robot-environment interface stiffness, k_x, k_y, k_θ.

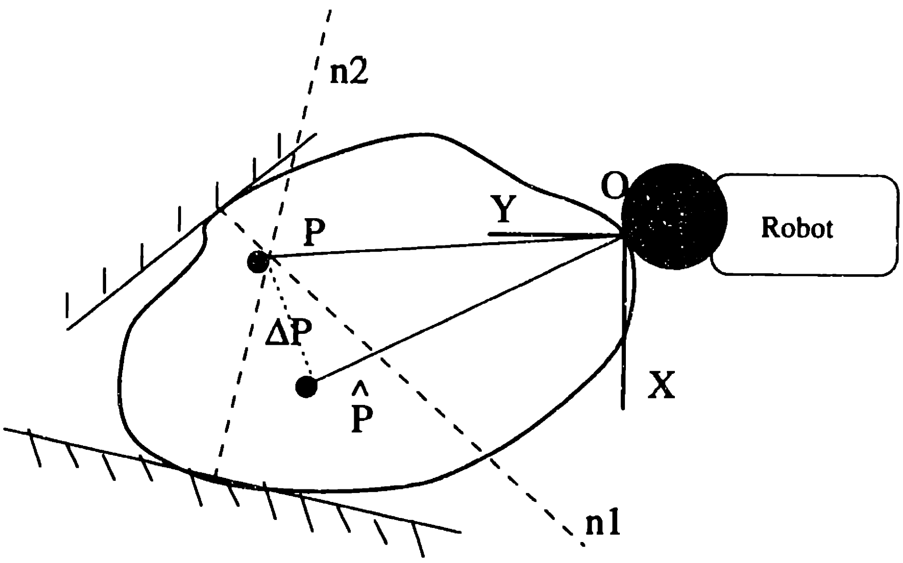

Figure 5.7: Multiple-Point Contact Model

From Figure 5.7, define point P as the true instantaneous center of rotation, herein also referred to as the vector P from the origin of the task coordinate system centered at the end of the robot, O. An estimate of the true point of rotation, $\hat{P}$, is known, and P lies at an unknown orientation ΔP from $\hat{P}$.

During small amplitude, pure rotations about P, the normal reaction forces exerted on the body remain constant. Rotations about any other point cause a change in the normal reaction forces due to motion that extends into one of the surfaces. If the body undergoes pure rotation about any $\hat{P}$, the change in reaction forces is equal the the change in reaction forces caused by an equivalent translation and rotation about P. Since the rotational motion about P produces no effect on the reaction forces, the equivalent change in normal forces is due merely to the equivalent pure translation about P. Therefore, if the change in reaction forces and the equivalent translation about P can be determined from a known rotation about $\hat{P}$, the unknown orientation ΔP can be located.

Forces normal to the constraint surfaces act in the constrained motion space while the forces tangent to the constraint surfaces, including friction, act in the admissible motion space. Filtering the force measurements to reflect only the constrained motion space requires projecting a zero moment about the instantaneous center of rotation. From Figure 5.7, the measured moment, M_s, and forces, F_N, F_T,s are related by

$$M_s = F_N \times P + F_T \times R \tag{5.11}$$

where each F in the following analysis reflects a vector of x and y components unless specified otherwise. R is the vector from O to the point of intersection of the surface tangents. Likewise, the moment at P is

$$M_p = F_T \times (R - P) \tag{5.12}$$

Therefore

$$M_s = M_p + F_{fs} \times P \tag{5.13}$$

for measured force

$$F_{fs} = F_N + F_T \tag{5.14}$$

To filter out the frictional effects, one of the following conditions must hold,

$$M_p = 0 \tag{5.15}$$

or

$$M_s = F_N \times P \tag{5.16}$$

It follows then that F_{Tx} and F_{Ty} satisfy the equations

$$\begin{aligned} F_{Ty}^2\left(1+p^2\right) &= F_{Ty}\left(2cp + pF_{fsx} + F_{fsy}\right) - \left(M^2 + cF_{fsx}\right) && (5.17) \\ F_{Tx} &= F_{Ty}p - c && (5.18) \end{aligned}$$

for $p = \frac{P_x}{P_y}$ and $c = \frac{M_c}{P_y}$. Subtracting F_T from F_{fs} removes those forces not acting through the center of rotation and hence indicates the boundary between admissible and constrained motion space. The remainder of the discussion assumes that this filter has already been performed.

5.4.2 Theoretical Framework

From the magnified vectorial view in Figure 5.8, an instantaneous rotation $d\theta$ about $\hat{P}$ causes a translation $dP = |\Delta P| d\theta$ of the point P. The equivalent forces on the body are given by

$$\begin{aligned} F_x - F_{xo} &= k_x dP_x = k_x |\Delta P| \cos\bar{\theta} d\theta && (5.19) \\ F_y - F_{yo} &= k_y dP_y = k_y |\Delta P| \sin\bar{\theta} d\theta && (5.20) \end{aligned}$$

where F_o indicates the preloading from initial contact between the body and the environment. Note that as P could lie at any orientation from $\hat{P}$, $\bar{\theta}$ need not be small in magnitude.

In order to estimate the instantaneous center of rotation, the goal is to determine $|\Delta P|$ and $\bar{\theta}$. Consistent with the dynamic arguments, rotational dither is used instead of translational such that the amplitude A now indicates radians. The force equations become:

$$\begin{aligned} F_x - F_{xo} &= k_x |\Delta P| A \cos\bar{\theta} \sin\omega t && (5.21) \\ F_y - F_{yo} &= k_y |\Delta P| A \sin\bar{\theta} \sin\omega t && (5.22) \end{aligned}$$

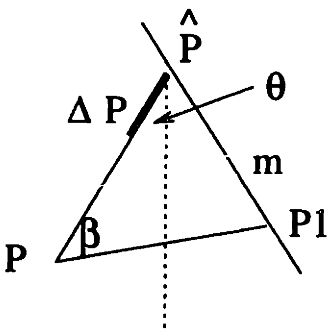

Figure 5.8: Construction of Dither Axes

Computing the root mean square for a given $|\Delta P|$ and $\bar{\theta}$,

$$\begin{aligned} RMS_x &= \left[\int_0^{2\pi\omega} (F_x - F_{xo})^2 dt\right]^{1/2} && (5.23) \\ &= \sqrt{\frac{\pi}{\omega}} k_x |\Delta P| A \cos\bar{\theta} && (5.24) \\ RMS_y &= \sqrt{\frac{\pi}{\omega}} k_y |\Delta P| A \sin\bar{\theta} && (5.25) \end{aligned}$$

Choice of the dither axis must be performed carefully to ensure that the desired variables can be determined. The limitation exists due to the inherent correlation between ΔP and $\delta\bar{\theta}$. Figure 5.8 illustrates the construction of an appropriate choice of dither axes. From the point $\hat{P}$ choose a small angle β and move along that direction for a small distance m chosen according to the scale of the part. Call that new point P_1. For $\beta \ll 1$, $\angle\hat{P}PP_1 = \beta$ and $\bar{\theta}_1 = \bar{\theta} + \beta$. Rotational dither operations are performed about the points $\hat{P}$ and P_1 with the same amplitude A. The corresponding root mean square values are determined and the following ratios are formed.

$$r_x = \frac{RMS_x(\bar{P}_1)}{RMS_x(\hat{P})} = \frac{|\bar{P}_1|\cos(\bar{\theta}+\beta)}{|\Delta P|\cos\bar{\theta}} \qquad (5.26)$$

$$r_y = \frac{RMS_y(\bar{P}_1)}{RMS_y(\hat{P})} = \frac{|\bar{P}_1|\sin(\bar{\theta}+\beta)}{|\Delta P|\sin\bar{\theta}} \qquad (5.27)$$

$$r = \frac{r_x}{r_y} = \frac{|\bar{P}_1|\cos(\bar{\theta}+\beta)|\Delta P|\sin\bar{\theta}}{|\bar{P}_1|\sin(\bar{\theta}+\beta)|\Delta P|\cos\bar{\theta}} = \frac{\tan\bar{\theta}}{\frac{\beta+\tan\bar{\theta}}{1-\beta\tan\bar{\theta}}} \qquad (5.28)$$

For known r and β,

$$\tan\bar{\theta} = \frac{(1-r) \pm \sqrt{(r-1)^2 - 4\beta^2 r}}{2\beta} \qquad (5.29)$$

This first set of two dither operations determines the angle $\bar{\theta}$. To solve for the length $|\Delta P|$ one more dither operation is required at a chosen distance δP along the $\bar{\theta}$ direction, as illustrated in Figure 5.8.

$$|\Delta P| = \frac{\delta P}{1 - r_x} \tag{5.30}$$

As with the single point contact state, this technique does not require exact knowledge of the dynamic parameters of the system. Carefully chosen dither axes allows for decoupling of the unknown direction and magnitude calculation for the vector $\bar{P}$. Three dither operations are required as two values must be determined instead of one. Recursive methods can likewise be derived for the multiple contact states.

5.4.3 Simulation

As with the single point contact algorithm, a simulation was conducted on MATLAB to verify the theoretical equations. At the start only knowledge of the size of the box and initial forces was provided. All other parameters were derived based on the above equations. The forces were simulated based on a priori knowledge that the box was in a corner. This simulation was intended purely as a test of the control algorithm, without any further verification of its robustness or susceptibility to noise. Further real-time tests are required to fully consider all the practical considerations.

Figure 5.9 illustrates the results of the multiple contact simulation of the rotation of a box into a corner. The overall box motion is shown along with the trajectory of the estimated point of instantaneous rotation. A closer view of the trajectory of the actual and estimated points of rotation is also shown in Figure 5.10. The estimated values are nearly exact.

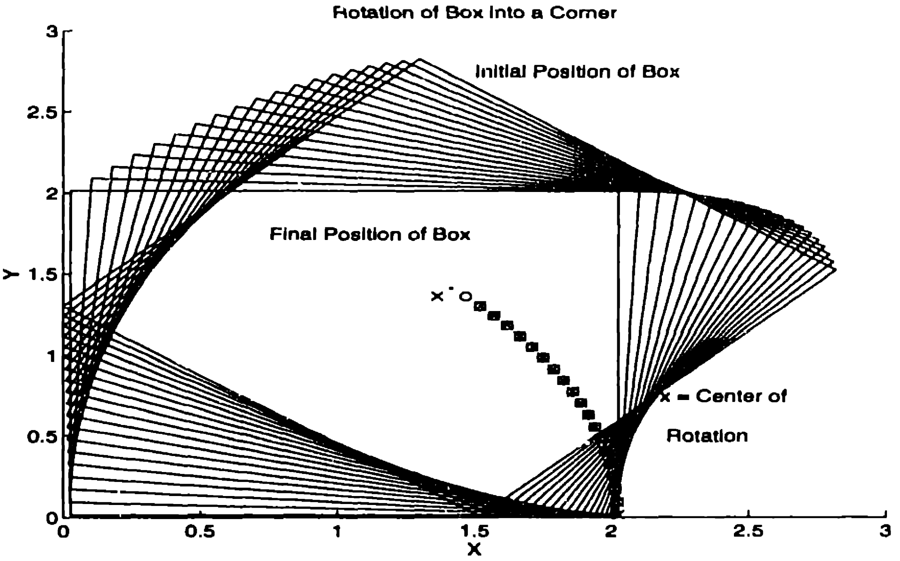

Figure 5.9: Simulation of Multiple Point Contact Assembly - Rotation of Box into Corner

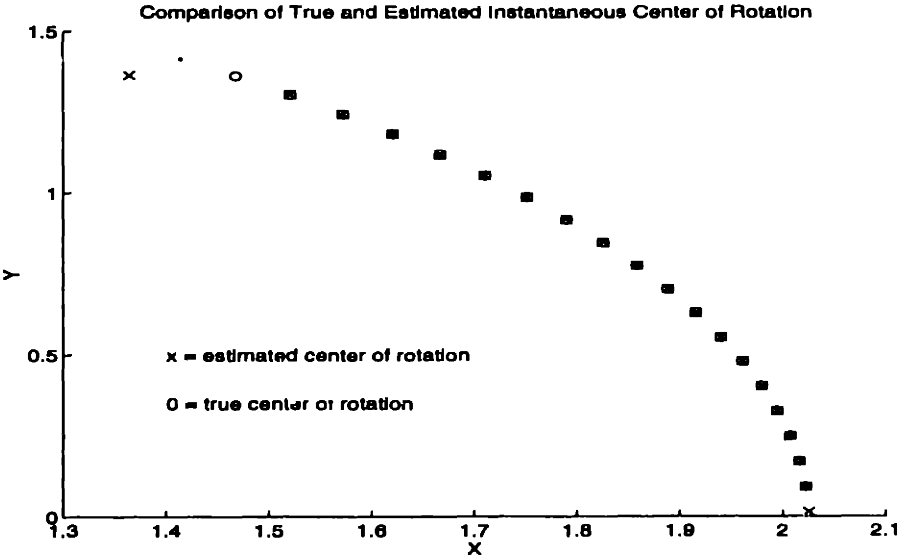

Figure 5.10: Actual versus Estimated Point of Instantaneous Rotation

Chapter 6

ACTIVE FORCE SENSING

Active force sensing exemplifies the adage 'together they are stronger than the sum of their two parts'. Matching of the needs of each component with the advantages of the other creates a powerful synergistic tool for robotic assembly in uncertain environments.

6.1 Contributions of Tuned Dither for Friction Suppression

Most assembly processes are influenced by friction. For many systems, any or none of an entire array of compensators, predictors, feedback and feedforward systems have been developed to decrease the noise and errors caused by this natural phenomenon. In many cases, however, these models require long on-line training, reference model identification, or exact knowledge of system parameters. Instead, use of dither does not rely on any exact models, and focuses on the dynamics of the system states directly. On-line tuning of the dither varies the compensation input to match the physical realities instead of indirectly tuning a system model which will then, directly or indirectly, determine the control inputs. The dither signal is added open loop to the robot motion, not interfering in any feedback dynamics, and due to its minimal magnitude, requires relatively very little actuation.

This dither algorithm is applicable to many assembly tasks involving similar contact states with the environment. As all interaction stiffnesses and parameters are defined globally to include effects from friction, the force sensor, and the robot, there is effectively no assumption that only one point of contact is made or that contact lies within a single plane. Incorporation of a dither motion in three degrees of freedom would be effective for friction suppression with multiple contact points.

The dither algorithm is effective for the entire region of nominal robot velocities and dither characteristic velocities. The only possible exception occurs when these values are relatively equal. Yet even in this case the friction forces are still slightly reduced from the situation without dither, and the dither parameters are easily adjusted to prevent this problem. At high robot velocities and low dither velocities, a nonzero average friction force remains, but is less than without the dither. With the flexibility of the dither actuators relatively high dither velocities can also be obtained. The most promising result is that for dither velocities greater than the robot velocity, the average friction force approaches zero. With the inclusion of the tuning mechanism, no assumptions need be made about the relative size of these velocities a priori. The dither parameters are naturally drawn to a local minimum for the friction forces.

It has been assumed that the friction model does hold for the assembly materials involved, including hard plastics and metals. Softer, more ductile materials may exhibit other properties which need to be addressed. Delicate pieces of metal or plastic, such as very thin electrical chip legs, still adhere to this physical model. Their shape is manifested through changes in their interaction stiffness and damping.

6.2 Analysis of Force Feedback Algorithm

6.2.1 Assumptions

The surface tracking algorithm incorporates many assumptions concerning the nature of the force readings and the physical system which must be justified. These assumptions can be divided into three sections depending on their source.

- Physical System
    1. Calculations are local and satisfy the persistent excitation condition
    2. Sampling times match with zero phase lags
- Mathematics
    1. Measured forces provide adequate information
    2. Model estimate is physically realistic
- Dither Operation
    1. Elastic response in both tangential and the normal directions
    2. Contact maintained through entire operation
    3. Symmetric motion throughout dither
    4. Motion is periodic
    5. Force measurements accurate with minimal delay
    6. Robot actuator bandwidths taken into consideration

Assumptions about the physical system arise from the need for a minimum subset of knowledge about the task geometry. In order to ensure adequate information is known for parameter estimation, the persistent excitation condition must be satisfied. This is achieved through the use of more than one dither operation at prescribed angles. One advantage of the dither is that the control motion can be contained to a very local region and still satisfy the persistent excitation condition. The only adverse assumption here is that the uncertainties to be accounted for are relatively small. When used for tracking completely unknown surfaces, large, sudden deviations from the expected trajectory may not be correctly recognized. Only previous knowledge can prevent this. Likewise, ensuring that the force sensor and encoder sampling times are matched with the dither frequency requires adequate forethought. For robotic assembly tasks, such foreknowledge is expected.

Mathematically, the algorithm relies on force feedback information that correctly represents the current dynamic state of the system. With the hybrid controller and friction suppression mechanisms, the force feedback signals are regulated to remain as smooth an constant as possible. As long as the tracking operation is maintaining the trajectory signal close to the actual surface, these signals remain accurate, and the two operations continuously work together for optimal performance. The derivation of the friction model is based on much work on the mature of friction on micro- and macroscopic levels. Likewise, they have been used to successfully predict friction in other studies. The friction model which forms the basis for this work can be considered accurate.

The assumptions concerning the dither operation are more closely related to the kinematics of the system and the choice of dither parameters. The six assumptions listed above can be divided further into the first four which the dither amplitude addresses, and the remaining two which the dither frequency addresses. The first four assumptions depend on the nature of the contact between the end effector and the robot. Contact must be maintained throughout the operation, and the dither motion must be periodic and continuous. To address the issue of elastic response and maintaining contact, upon contact a preload is established and maintained through force control. Based on the estimated interaction stiffness from the friction suppression operation, a maximum value is placed on the dither amplitude, such that at the extreme points of dither motion, contact is not lost. Otherwise the amplitude is chosen based on a multiple of the friction suppression dither value. The theoretical derivation assumes that the dither motion will be periodic and maintain a symmetric sinusoidal form. In reality, the position controller is accurate enough to create a periodic motion, but the nature of the contact often prevents the actual motion from maintaining symmetry with respect to the amplitude. To account for this, the expression for determining α_o given in equation 5.8 above is modified to include the maximum distance traveled on each side of the dither stroke. Working out the calculations for $A_1 \neq A_2$, the final equation becomes

$$\alpha_o = \frac{R_1 A_2 \delta\alpha_2 - R_2 A_1 \delta\alpha_1}{R_2 A_1 - R_1 A_2} \tag{6.1}$$

With this simple modification and maintenance of a force preload, the first set of dither assumptions are met. In addition, for extremely stiff materials, the dither angles can be chosen to lie more closely parallel to the tangent than to the normal, as the effective stiffness in the former region is less than the latter.

The remaining assumptions relating to the dither frequency require that the bandwidth and sampling time limitations of the sensors and actuators be appropriately taken into consideration. This requirement is common practice in control system implementation and was appropriately taken into consideration.

6.2.2 Validity

Accurately implementing any parameter estimation technique requires that the persistent excitation condition be met. Incorporating two dither operations in nonparallel directions is adequate in a planar vector space for satisfying this condition. The advantage of the dither operation is that this task space is explored within a localized region with very little overall motion. These localized measurements are sufficient for updating the robot trajectory and in series, determining the entire global trajectory. Within the actual computer code, the surface is characterized by the value of its tangent. Following the dither operation, this tangent value is adjusted by the calculated amount, and hence recorded in the overall knowledge of the position controller. This indirectly works as a feedforward mechanism to compensate once for a single surface directional change without having to continually dither on a straight surface.

The algorithm relies only on the measured force values and the motion of the robot to estimate the surface. As these measurements are taken in real-time, they are more accurate than any estimated parameter and do not assume that the robot has exactly followed the desired trajectory. The calculation is relatively simple, maximizing the use of its measurements. In total, the surface tracking algorithm provides a compact, simple method for utilizing force feedback and minimal control action to achieve a fundamental robotic assembly operation.

This algorithm was originally intended to compensate for uncertainties in an estimated surface. However, it could be employed to track a completely unknown surface, given that the trajectory is continuous and has a moderate to low curvature. In this case, the dither operation would be employed much more frequently. Along sections of relatively constant slope, the operation would only have to run at the beginning or end of each section. Anticipation of possible problems can also be included in the algorithm, such as rapid velocities due to harsh impacts. Compensation in adjusted speeds can be made depending on the exact environment and parts involved as in [Youcef-Toumi and Gutz 89]. Likewise, the force controller would help compensate for such errors.

Just as with the friction suppression algorithm, one can envision dither parameters tuned to optimize the surface tracking operation. Such compensation would have to consider the interaction stiffness, surface roughness, actuator bandwidths, and the quality of the force feedback commands.

6.3 A Successful Combination

Friction suppression can successfully maintain contact forces at desired or measureable, well-behaved levels. These regular force signals improve the effectiveness of the surface tracking algorithm. As the robot controller gains better knowledge of its actual trajectory, the force controller and friction suppression dither must compensate for smaller errors, and hence produce even better signals. These better signals improve the surface tracking controller and the cycle begins again. Likewise, many of the assumptions and requirements from the surface tracking are met through friction suppression and vice versa. The dither for friction suppression is commanded along an estimate of the actual tangent. It is therefore assumed that this estimate is nearly perfect. On the other side, surface tracking relies very heavily on accurate force measurements and the ability to separate normal versus tangential forces.

The actual mechanisms for performing the two tasks do not act simultaneously. Friction suppression is a dynamic operation, running any time the robot is undergoing directional motion. Determination of the surface tangent, however, occurs during a discrete, stationary operation, not continually during the robot motion. It is therefore actually the results of the surface tracking combined with the actuation of the friction suppression which produces the desired results.

In a similar manner, the two mechanisms address different, yet complementary purposes. Force feedback information is the single source of information for both the friction suppression and the surface tracking. As such, the form and validity of this signal is of primary importance to active force sensing. Analysis was performed on the nature of the signal and the root causes of the problems with the signal. Then, appropriate measures were taken to develop the friction suppression and surface tracking algorithms to control the form of the force feedback signal in an effective and straight forward manner. The algorithms perform complementary functions on this level as well.

Both algorithms do employ a dither operation, yet with very different needs. The friction suppression requires a high frequency signal at very low amplitude. It simply supplies continued motion without regard to signal phase or noise. Surface tracking requires much more signal regulation and limited phase lag as the actual robot positioning is directly involved in the calculations. Ideally though, the two signals could be superimposed upon one another and still remain effective. Yet as dither for the friction suppression is a dynamic operation, and the dither for surface tracking is static, the signals are used independent of each other.

Chapter 7

CONCLUSIONS AND FUTURE RECOMMENDATIONS

7.1 Conclusions

This initial work demonstrates the needs and priorities for the characteristics of an accurate robotic assembly control structure in uncertain environments. The advantages of local versus global measurements for accurate tracking was demonstrated as well as the need for quick, concise information which satisfies the persistent excitation condition. On-line trajectory generation and adaptive control requires minimal calculations and a minimum number of parameters to estimate. Use of the dither operation in conjunction with force feedback is capable of estimating a single localized, required variable which contains all the required information for control. Simple calculations can be performed on-line without sacrificing the persistent excitation condition.

Preliminary testing shows initial promise for the applicability and effectiveness of this technique. Although friction cannot be precisely modeled or compensated for, control and measureability of its effects has been achieved, along with minimization of its signal fluctuations. In uncertain and large scale environments, precise modeling is not even feasible, nor necessary. Most importantly, this system is computationally unintensive and self-tuning.

7.2 Future Recommendations

As a stepping stone, this thesis points to much future work to improve the active force sensing algorithm and result in a robust, useful control system for assembly processes. The first step is further confirmation of the surface tracking results and expansion of experimentation towards multiple point contact assembly operations. Due to the limitations of the actuator bandwidths, a device which localizes the dither motion at the robot end effector and greatly increases the frequency capability, will be built. Further testing will include a model for different material, determination of range of errors which the dither can overcome, and specific applications.

An effective surface tracking controller can likewise be improved through the addition of a self-tuning mechanism for the surface tracking dither parameters. Although theoretically the effectiveness of the algorithm does not depend on this tuning, as with the friction suppression algorithm, practical limitations should be taken into account. This parameter optimization routine will take into consideration the relative stiffness of the interaction, and the amount of data required for an accurate estimate. Algorithm limits can also be found for the curvature of the surface, the level of signal noise, and force thresholds. Multiple point contact assembly tasks hold much promise for flexibility in controller structure. The technique presented will be further verified through experimentation. Coupled with this flexibility is the ability to detect and adjust to discrete changes in surface curvature or contact state. The relationship between the force feedback and such discrete events must be identified. Once a robust general control structure is in place, work will lead towards a complete adaptive control scheme which improves through repetitive tasks and can more easily handle completely unknown trajectories.

Expansion and acommodation for industrial applications must then be included. The detection of discrete events such as sharp corners increases the range of algorithm applicability. Likewise, as many assembly tasks are repetitive, the capability to remember and incorporate frequent similar corrections into the nominal trajectory would be extremely valuable.

Bibliography

[Armstrong-Helouvry 91] B. Armstrong-Helouvry. *Control of Machines with Friction* Kluwer Academic Publishers, Boston. 1991.

[Asada and Li 92] H. Asada and S. Li. "Automated Robotic Assembly Using a Vibratory Work Table: Optimal Tuning of Vibrators Based on the Taguchi Method," *Proc. Japan-USA Sumposium on Flexible Automation,* vol. 2, 1992.

[Asada and Slotine 86] H. Asada and J.J. Slotine. *Robot Analysis and Control* Wiley and Sons, 1986.

[Bay and Hemami 90] J.S. Bay and H. Hemami. "Dynamics of a Learning Controller for Surface Tracking Robots on Unknown Surfaces," *IEEE Trans. on Automatic Control,* vol. 35, no. 9, pp. 1051-1054, 1990.

[Boothroyd, Poli, and Murch 82] G. Boothroyd, C. Poli, and L. Murch. *Automatic Assembly* Marcell Dekker, Inc. New York. 1982.

[Carpender, et. al. 91] P.W. Carpenter, et. al. "The Optimization of Compliant Walls for Drag Reduction" *Recent Developments in Turbulence Management* K.S.Choi ed. Kluwer Academic Publishers, Netherlands. pp. 195-221, 1991.

[Demey and DeSchutter] S. Demey and J. DeSchutter. "Enhancing Surface Following with Invariant Differential Part Models," *Proc. IEEE Conf. on Robotics and Automation,* pp. 668-673, 1994.

[Dupont 91] P.E. Dupont. "Avoiding Stick/Slip in Position and Force Control Through Feedback," *Proc. 1991 Inter. Conf. on Robotics and Automation.* IEEE, pp.1470-1476, 1991.

[Hamill and McBride 95] O.P. Hamill, D.W. McBride. "Mechanoreceptive Membrane Channels," *American Scientist,* vol.83, no. 1, pp. 30-37, 1995.

[Ipri and Asada 94] S.L. Ipri and H. Asada. "Force-Guided Robotic Assembly Using Tuned Dither and Recursive Parameter Estimation," *Proc. Dynamic Systems Measurement and Control, 1994 ASME WAM,* vol. 2, pp. 857,862, Chicago 1994.

[Ipri and Asada 95] S.L. Ipri and H. Asada. "Tuned Dither for Friction Suppression During Force-Guided Robotic Assembly," Submitted to *1995 IROS Conference.* Pittsburgh, August 1995.

[Johnson and Lorenz 91] C.T. Johnson, and R.D. Lorenz. "Experimental Identification of Friction and Its Compensation in Precise, Position Controlled Mechanisms," *Proc. IEEE Industry Appl. Society Annual Mtg,* pp. 1400-1406, 1991.

[Lee and Asada 94] S. Lee and H. Asada. "Assembly of Parts with Irregular Surfaces Using Active Force Sensing," *Proc. IEEE Int. Conf. on Robotics and Automation,* 1994.

[McCarragher] B.J. McCarragher. "A Discrete Event Dynamic Systems Approach to Robotic Assembly Tasks," Ph.D. Thesis, Massachusetts Institute of Technology, 1992.

[Oldenburger and Boyer 62] R. Oldenburger and R.C. Boyer. "Effects of Extra Sinusoidal Inputs to Nonlinear Systems," *Journal of Basic Engineering,* Dec. 1962.

[Peshkin 90] M.A. Peshkin. "Programmed Compliance for Error Corrective Assembly," *IEEE Trans. on Robotics and Automation,* vol. 6, no. 4, pp. 473-482, 1990.

[Raibert and Craig 81] M.H. Raibert and J.J. Craig. "Hybrid Position/Force Control of Manipulators," *AMSE Journal Dynamic Systems Measurement and Control,* pp. 126-133, June 1981.

[Russell 90] R. A. Russell. *Robot Tactile Sensing* Prentice Hall, Sydney. 1990.

[Takahashi, Ogata, and Muto 93] T. Takahashi, H. Ogata, S. Muto. "A Method for Analyzing Human Assembly Operations for use in Automatically Generating Robot Commands," *IEEE Proc.* pp. 695-700, 1993.

[Townsend and Salisbury] W.T. Townsend, J.K. Salisbury. "The Effect of Coulomb Friction and Stiction on Force Control," *Proc. IEEE Conf. on Robotics and Automation,* pp. 883-889, 1987.

[Wang, Kumar, and Abel 92] Y. Wang, V. Kumar, and J. Abel. "Dynamics of Rigid Bodies Undergoing Multiple Frictional Contacts," *Proc. of IEEE Conf. on Robotics and Automation,* pp. 2764-2769, 1992.

[Weaver 59] W. Weaver. "Dither," *Science,* vol. 130, p. 301, 1959.

[Whitney 77] D.E. Whitney. "Force Feedback Control of Manipulator Fine Motions," *ASME Journal Dynamic Systems Measurement and Control,* pp. 91-97, June 1977.

[Whitney 82] D.E. Whitney. "Quasi-Static Assembly of Compliancy Supported Right Parts," *ASME J. Dynamic Systems, Measurement, and Control,* vol. 104, 1982.

[Xu and Paul 90] Y. Xu and R. Paul. "A Robot Compliant Wrist System for Automated Assembly," *IEEE,* pp. 1750-1755, 1990.

[Yang 95] B. Yang. "A Progressive Learning Approach ...," Ph.D. Thesis, Massachusetts Institute of Technology, 1995.

[Yoshikawa 93] T. Yoshikawa. "Hybrid Control Theory of Robot Manipulators" *Proc. Sixth Int. Symposium on Robotics Research,* 1993.

[Youcef-Toumi and Gutz 89] K. Youcef-Toumi and D.A. Gutz. "Impact and Force Control," pp. 410-416, 1989.